Feasibility Study on the Use of Ultrasonic Guided Waves for the In-Line Inspection of Axial Cracks in Large Diameter Cast-Iron Water Pipes

by

Baptiste GAUTHIER

THESIS PRESENTED TO ÉCOLE DE TECHNOLOGIE SUPÉRIEURE
IN PARTIAL FULFILLEMENT FOR A MASTER'S DEGREE
WITH THESIS IN MECHANICAL ENGINEERING
M. A. Sc.

MONTREAL, DECEMBER 10, 2018

ÉCOLE DE TECHNOLOGIE SUPÉRIEURE
UNIVERSITÉ DU QUÉBEC

BOARD OF EXAMINERS

THIS THESIS HAS BEEN EVALUATED

BY THE FOLLOWING BOARD OF EXAMINERS

Prof. Pierre Bélanger, Thesis Supervisor
Department of mechanical engineering at École de technologie supérieure

Prof. François Blanchard, President of the Board of Examiners
Department of electrical engineering at École de technologie supérieure

Prof. Ricardo Zednik, Member of the jury
Department of mechanical engineering at École de technologie supérieure

THIS THESIS WAS PRENSENTED AND DEFENDED

IN THE PRESENCE OF A BOARD OF EXAMINERS

ON DECEMBER 5, 2018

AT ÉCOLE DE TECHNOLOGIE SUPÉRIEURE

ACKNOWLEDGMENT

I first would like to thank my research advisor Prof. Pierre Belanger for his constant support, his precious advices and his patience in the context of my thesis project but also for all the events and side projects in which he involved me. It was a real pleasure to work with him as a real partner and with his full confidence.

A very warm and special thanks to all my colleagues: Frédéric Dupont, Guillaume Boivin, Aurélien Thon, Nicolas Tremblay the 12th, Timothé Falardeau, Victor Cerda Carvajal, Sevan Bouchy, Geoffrey Veit, Arthur Chaton, Anthony Moulins, Daniel Pereira, Shreyank Gupta, Mathieu Lessard and Cherif Azzaz. You were a real cornerstone of all the work accomplished and I spent amazing moments with all of you.

This project was made possible thanks to our industrial partner Pure Technologies LTD. A special thanks to Xiangjie Kong, Vice President Research & Development for his support during this project.

This master's degree would not have been possible without the partnership between my engineering school in France, Arts et Métiers ParisTech, and École de Technolgie Supérieure, so I would like to be grateful to all the people involved in the preservation and development of this relationship.

Finally, I would have not been able to put any foot in Canada without the unconditional support of my family. Not matter how far you were, thanks sincerely for making this adventure possible!

To my uncle.

Étude de faisabilité sur l'utilisation d'ondes guidées ultrasonores pour l'inspection interne de fissures axiales dans des conduites d'eau en fonte de grand diamètre

Baptiste GAUTHIER

RÉSUMÉ

Les ondes guides ultrasonores sont largement utilisées pour l'inspection de tout type de conduites. Cette technologie repose sur la propagation d'une onde mécanique sur de grandes distances grâce à des réflexions successives sur les frontières de la structure (qu'elle soit de type plaque ou cylindrique) qui agit alors comme guide d'onde. Généralement, un collier de traducteurs ultrasonores est utilisé pour l'émission de l'onde mais aussi pour la réception du signal issu de l'interaction de l'onde avec un potentiel défaut. Par cette méthode qui est largement commercialisée on peut détecter précisément de nombreuses défectuosités comme de la corrosion ou des fissures. Cependant, ce type d'inspection nécessite l'accès à la surface externe de la conduite, ce qui peut dans le cas des conduites d'alimentation en eau se révéler difficile puisqu'elles sont généralement enterrées sous les routes. Des outils d'inspection internes sont alors souvent utilisés pour ce type de structures et font appel à des technologies aussi variées que la magnétoscopie, l'inspection par courants de Foucault ou bien encore l'inspection ultrasonore. Les robots d'inspection interne conventionnellement utilisés sont adaptés à la détection de fuite mais requièrent une durée d'inspection plus longue et couteuse lorsqu'il s'agit de détecter précisément de petits défauts. Enfin, les défaillances observées dans les conduites d'eau en fonte de grand diamètre sont le plus souvent reliées à la propagation de fissures axiales initiées pas de la corrosion localisée ou des contraintes thermiques trop importantes.

Dans ce projet, on s'intéresse à la faisabilité de combiner la précision des technologies d'ondes guidées ultrasonores à la polyvalence des robots d'inspection internes qui permettent un contrôle facile et rapide de conduites sur plusieurs kilomètres. Une méthode d'inspection, appuyée par des simulations éléments finis a été proposée et utilise une couronne de traducteurs espacés de manière égale et qui serait montée sur le robot. Le mode fondamental d'ondes guidées (dans une structure cylindrique ou son homologue dans une structure plaque) relatif au déplacement hors plan de la perturbation a été étudié. Les simulations et la méthode proposée ont ensuite été confrontés à leur étude expérimentale sur un échantillon de tuyau en fonte de 24 pouces fourni par le partenaire industriel. À la lumière des résultats obtenus, une conclusion sur la faisabilité de l'inspection par ondes guidées ultrasonores de conduites d'eau en fonte de grande dimension ainsi que des pistes pour les travaux futurs ont été formulées.

Mots clés : Ondes guidées, Inspection interne, Fonte, Conduites d'eau

Feasibility Study on the Use of Ultrasonic Guided Waves for the In-Line Inspection of Axial Cracks in Large Diameter Cast-Iron Water Pipes

Baptiste GAUTHIER

ABSTRACT

Ultrasonic guided waves are commonly used for the inspection of pipelines. The inspection method basically consists of the propagation of a wave along a long distance thanks to multiple reflections between the boundaries of a structure which act as a waveguide. Transducers mounted on the outer surface of the pipe via a collar are used for the insonification, as well as for the measurement of the wave, which is reflected at potential defect locations. This method allows us to detect important flaws, such as corrosion and cracks, and is now commercialized. However, this technique requires access to the pipe's outer surface, which is typically possible for oil and gas pipelines, but harder for water networks, that are usually buried under roads. On the other hand, pipe inspection gauges (PIGs) are used for the in-line inspection (ILI) of water pipes using magnetic flux leakage (MFL), eddy current (EC), or ultrasonic testing (UT) technologies. These technologies are well suitable for leak detection, but inspecting smaller defects often requires a longer time of acquisition or heavy and expensive hardware. Additionally, pipe failures in large diameter cast-iron water pipes are often associated with the propagation of axial cracks initiated by corrosion or thermal stress.

In this project, we study the feasibility of combining the powerful detection abilities of guided waves with the versatility of PIGs that allow a fast and easy way to inspect the integrity of water mains, over several kilometers, for the inspection of axial cracks in large diameter pipes. An inspection method, assessed by finite element (FE) simulations, was proposed using an array of equally spaced transducers that would be attached to the PIG. The use of the fundamental out of plane pipe or similar plate mode was investigated. The proposed method was simulated and tested experimentally on a 24-inch pipe sample provided by the industrial partner. In light of the obtained results, a conclusion on the feasibility of the use of ultrasonic guided waves for the in-line inspection of large diameter water pipe is given and recommendations, as well as interesting avenues for upcoming work, are formulated.

Keywords: Guided Waves, In-Line Inspection, Cast Iron, Water Pipes

TABLE OF CONTENTS

Page

INTRODUCTION 1

CHAPTER 1 THEORETICAL BACKGROUND AND LITERATURE REVIEW 3
1.1 Fundamentals of Ultrasonic Wave Propagation 3
1.1.1 Mechanical Bulk Waves Propagation in Solids 3
1.1.1.1 1D Formulation 4
1.1.1.2 3D Formulation 5
1.1.1.3 Interactions at boundaries 8
1.1.1.4 Attenuation 9
1.1.2 Guided Waves Propagation in Solid Plate-Like Structures 9
1.1.2.1 Shear-Horizontal Waves 10
1.1.2.2 Lamb Waves 13
1.1.3 Guided Waves Propagation in Solid Pipe Structures 16
1.1.3.1 Torsional Pipe Modes 17
1.1.3.2 Longitudinal Pipe Modes 18
1.1.3.3 Flexural Pipe Modes 19
1.1.3.4 Plate Analogy 20
1.1.4 Conclusion on Wave Propagation and Ultrasound 21
1.2 Water Pipes Failures 22
1.2.1 Failures Causes of Cast-Iron Water Pipes 22
1.2.1.1 Manufacturing Process Causes 22
1.2.1.2 Environmental Causes 23
1.2.1.3 Utilization and Human Causes 23
1.2.2 Failures Modes of Cast-Iron Water Pipes 24
1.2.2.1 Small Pipes Failure Modes 24
1.2.2.2 Large Diameter Pipes Failure Modes 25
1.2.3 Conclusion on Water Pipes Failures 26
1.3 Water Pipes In-Line Inspection Solutions 26
1.3.1 Magnetic Flux Leakage (MFL) 27
1.3.2 Ultrasonic Testing 27
1.3.2.1 Piezoelectric Transducers 27
1.3.2.2 EMAT 28
1.3.3 Eddy Current Testing 29
1.3.4 Conclusion on Water Pipes In-Line Inspection Solutions 29

CHAPTER 2 EVALUATING THE INSPECTION METHOD BY FINITE ELEMENT SIMULATIONS 31
2.1 The inspection method 31
2.1.1 Overview of the process 32
2.1.2 Step by step measurement method 33
2.2 Simulation parameters 34

2.2.1 Elements type 34
2.2.2 Elements size 34
2.2.3 Time increment 35
2.3 Two-dimensional simulation 35
2.3.1 Studied case 35
2.3.2 Model 36
2.3.3 Results 37
2.4 Three dimensional simulations 38
2.4.1 Model 39
2.4.2 Results and imaging 40
2.5 Conclusion on the inspection method and its assessment using FE simulations 44

CHAPTER 3 EXPERIMENTAL TESTS 45
3.1 Propagation of guided waves in the coated pipe 46
3.1.1 Dry tests 46
3.1.2 Semi-immersed tests 47
3.2 Inspection of a machined groove and first conclusions 48
3.2.1 Inspection of a machined groove reproducing the simulated case 49
3.2.2 Measurement of the ultrasonic guided wave velocity in a simple cast-iron plate 51
3.2.3 Measurement of the guided wave speed in the pipe using transduction on each side of the pipe 54
3.2.4 First conclusions on the feasibility of the proposed method 55
3.3 Use of an ultrasonic array 55

CONCLUSION 59

BIBLIOGRAPHY 61

LIST OF FIGURES

Page

Figure 1.1 Deformation induced in a solid medium by the propagation along the x-axis. a. a longitudinal bulk wave (or P-wave or L-wave) and b. a shear bulk wave (or S-wave or transverse wave) 7

Figure 1.2 Interactions of an incident mechanical wave at a. a solid/solid interface and b. a liquid (non-viscous)/solid interface 8

Figure 1.3 Propagation of a Shear-Horizontal (SH) guided wave along x between two free surfaces at $y = b$ and y $= -b$ 11

Figure 1.4 Phase velocity dispersion curves of SH modes in a 22 mm thick cast-iron plate (E = 78.3 GPa, ν = 0.17, ρ = 6900 kg/m^3), frequency range is 0-5MHz. Computed using the GUIGUW software (Bocchini, Marzani, & Viola, 2011) 12

Figure 1.5 Group velocity dispersion curves of SH modes in a 22 mm thick cast-iron plate (E = 78.3 GPa, ν = 0.17, ρ = 6900 kg/m3), frequency range is 0-5MHz. Computed using the GUIGUW software (Bocchini et al., 2011) 13

Figure 1.6 Propagation of Lamb guided waves along x between two free surfaces at $y = b$ and $y = -b$. Mode conversion (L-waves and SV-waves) occurs at each reflection on the surface 15

Figure 1.7 Phase velocity dispersion curves of Lamb modes in a 22 mm thick cast-iron plate (E = 78.3 GPa, ν = 0.17, ρ = 6900 kg/m3), frequency range is 0-500kHz. Computed using the GUIGUW software (Bocchini et al., 2011) 15

Figure 1.8 Group velocity dispersion curves of Lamb modes in a 22 mm thick cast-iron plate (E = 78.3 GPa, ν = 0.17, ρ = 6900 kg/m3), frequency range is 0-500kHz. Computed using the GUIGUW software (Bocchini et al., 2011) 16

Figure 1.9 Cylindrical coordinate set and pipe geometry 17

Figure 1.10 Phase velocity dispersion curves of pipe torsional modes in a 22 mm thick cast-iron pipe of diameter 309 mm (E = 78.3 GPa, ν = 0.17, ρ = 6900 kg/m3), frequency range is 0-500kHz. Computed using the GUIGUW software (Bocchini et al., 2011) 18

Figure 1.11 Phase velocity dispersion curves of pipe longitudinal modes in a 22 mm thick cast-iron pipe of diameter 309 mm (E = 78.3 GPa, ν = 0.17, ρ = 6900 kg/m3), frequency range is 0-500kHz. Computed using the GUIGUW software (Bocchini et al., 2011) 19

Figure 1.12 Phase velocity dispersion curves of pipe flexural modes (order 1 to 5) in a 22 mm thick cast-iron pipe of diameter 88 mm (E = 78.3 GPa, ν = 0.17, ρ = 6900 kg/m3), frequency range is 0-100kHz. Computed using the GUIGUW software (Bocchini et al., 2011).....20

Figure 1.13 Phase velocity dispersion curves of plate lamb modes (black) and pipe longitudinal modes in a 22 mm thick plate and cast-iron pipe respectively of diameter 44 (blue), 88 (green), 176 (yellow) and 352 (pink) mm (E = 78.3 GPa, ν = 0.17, ρ = 6900 kg/m3), frequency range is 0-2MHz. Computed using the GUIGUW software (Bocchini et al., 2011) 21

Figure 1.14 Small pipes (diameter < 380mm) failure modes. a. axial crack initiated at the bell, b. axial crack initiated due to corrosion pitting and pipe wall thinning, c. bell splitting, d. circumferential cracking, e. chain created corrosion 25

Figure 1.15 Large pipes (diameter > 380mm) failure modes. a. axial crack initiated at the bell, b. axial crack initiated due to corrosion pitting and pipe wall thinning, c. bell splitting, d. circumferential cracking, e. chain created corrosion 26

Figure 2.1 Transducers arrangement along a circular array on the PIG.....32

Figure 2.2 Inspection process.....33

Figure 2.3 Step by step measurement method.....34

Figure 2.4 Simplified 2D model.....36

Figure 2.5 Excitation signal. A 50kHz center frequency hann windowed tone burst.36

Figure 2.6 Wave propagation in the water and the cast-iron.....37

Figure 2.7 Dispersion curves from 2D FFT of measuring nodes displacement showing the propagation of A_0 and S_0 guided waves modes.....38

Figure 2.8 Simplified 3D model.....39

Figure 2.9 3D mesh (left) and 3D mesh with excitation nodes (right).....40

Figure 2.10 a. Measurement setup and crack location. b. Recorded time traces for node 3 excitation where node 3 excitation and node 2 direct path have been removed. c. Recorded times traces for node 5 excitation where node 5 excitation, node 4 and 6 direct path have been removed 42

Figure 2.11 a. Summation of back propagated signals for a given slice of the pipe and applied threshold. b. Pipe wall image resulting of the assembly of all slices, simulating an in-line inspection and showing the simulated crack 43

Figure 3.1 a. Pipe from which samples have been cut, b. Non-coated sample and c. Coated sample 45

Figure 3.2 Dry tests, a. at a given distance Z1 between the transducer and the laser vibrometer measurement, b. at a given distance Z2 between the transducer and the laser vibrometer measurement. The setup is shown on the left and the emitted and received signal on the right 46

Figure 3.3 Semi-immersed tests, a. Experimental setup, b. Emitted and measured signal, c. Frequency content of the emitted and received signal 48

Figure 3.4 Measurement setup for the inspection of the groove 49

Figure 3.5 Pitch-catch example of observed signals, transducer 1 is fired and signal is measured by transducer 3. 50

Figure 3.6 Measurement setup for pitch-catch tests on a cast-iron plate. 51

Figure 3.7 Pitch-catch measurement from transducer A to B 53

Figure 3.8 a. Measurement setup for the guided wave phase velocity measurement. b. Signals sent to transducer 1 and received by transducer 2.....54

Figure 3.9 Machined grooves on inner and outer surfaces of the pipe sample 56

Figure 3.10 Array setup above the groove under inspection.....56

Figure 3.11 Imaging results using the linear array. a. 100mm from the pipe surface. Image of the inner groove. Image width corresponds to probe aperture. b. 20 mm from the pipe surface. Image of the outer groove. Image width correponds to the probe aperture. c. 170 mm from the pipre surface.Image of the outer groove. Image corresponds to a 90 mm circumferential extent 57

LIST OF ABREVIATIONS

ALID	Absorbing Layer with Increasing Damping
EC	Eddy Current
EMAT	Electromagnetic-acoustic Transducer
FE	Finite Element
FFT	Fast Fourier Transform
FWHM	Full width at Half Maximum
ILI	In-Line Inspection
MFL	Magnetic Flux Leakage
NDT	Non-Destructive Testing
PIG	Pipeline Inspection Gauge
SH	Shear-horizontal
SV	Shear-vertical
TOF	Time-of-Flight
UT	Ultrasonic Testing
1D	One-Dimension
2D	Two-Dimensions
3D	Three-Dimensions

LIST OF SYMBOLS

δ_{ij}	Kronecker delta
$\frac{\partial}{\partial}$	Partial derivative
λ	First Lamé parameter
λ_{wl}	Wavelength
μ	Second Lamé parameter
ν	Poisson's ratio
Φ	Scalar potential
Ψ	Vector potential
ω	Angular frequency
ρ	Density
A	Wave amplitude
A_0	Initial wave amplitude
A_m	Antisymmetric mode of order m
V	Constant wave velocity
c_{ii}	Elasticity tensor value
V_{ph}	Phase velocity
V_g	Group velocity
cos	Cosine function
E	Young's Modulus
Hz	Hertz
k	Wavenumber

k_i	Wavenumber or wave vector component in direction of propagation i
k_s	Shear wavenumber
k_{SH}	Shear-horizontal wavenumber
$L(0,m)$	Longitudinal mode of order m
m	Meter
R	Reflection coefficient
s	Second
sin	Sine function
S_{ij}	Strain tensor
S_m	Symmetric mode of order m
SH_m	Shear-horizontal mode of order m
T	Transmission coefficient
tan	Tangent function
T_{ij}	Stress tensor
$T(0,m)$	Torsional mode of order m
$V_{\phi_{SH_m}}$	Phase velocity of SH guided wave mode of order m
$V_{g_{SH_m}}$	Group velocity of SH guided wave mode of order m
V_i	Incident wave velocity
V_L	Longitudinal wave velocity
V_T	Shear wave velocity
V_{tL}	Transmitted wave longitudinal velocity
V_{tT}	Transmitted wave transverse velocity

INTRODUCTION

Water networks installed in Northern America represent thousand of kilometers of aging pipes exposed, among many phenomena, to corrosion, ground movements and excavation work. Most of them are made of cast iron, which was considered, in the early nineties, as a standard and convenient material. Some of the pipes are more than a hundred years old and could last longer. However, it was noticed that the number of failures of this kind of pipe has been growing fast during the last decades so numerous non-destructive testing techniques (NDT) have been developed to inspect this kind of structure.

For large diameter pipelines, the typical failure mode is a crack ignition at the pipe bell due to thermal stress followed by axial propagation of the crack until the complete pipe failure. Some other reasons such as ground movements, excavation and corrosion could also lead to axial cracks but also to circumferential cracks.

NDT of water networks is a big issue since it involves huge costs when it is time to repair or replace a pipe due to excavation work and service disruption. Usually, NDT of pipeline is divided into two main fields: inspection from the outside and inspection from the inside. The range of inspection methods go from point-by-point inspections from the outside of the pipe to the use of pipeline inspection gauge (PIG) for in-line inspection (ILI) from the inside. The method which allows the longest inspection lengths relative to the cost of inspection is the use of ultrasonic guided waves (Lowe, Alleyne and Cawley, 1998). Contact transducer rings exciting and detecting ultrasonic guided waves were developed in the early two thousands and are now a common tool for rapid assessment of a pipeline condition. However, it still requires the excavation of a pipe section which is not always easy when it comes to water pipelines as they are often buried under roads.

Thus, in this project, the use of a PIG for the generation of ultrasonic guided waves in a water pipe wall was investigated. This would lead to the inspection and detection of small axial cracks in the pipe wall without any disruption of service and would not require excavation.

After a brief introduction to the theoretical background of the propagation of ultrasonic guided waves, a literature review of water pipe failures and existing solutions, a new in-line inspection method will be presented and assessed using numerical models and experimental validations.

CHAPTER 1

THEORETICAL BACKGROUND AND LITERATURE REVIEW

Assessing the feasibility of using ultrasonic guided waves for in-line inspection of large diameter water pipes requires a solid understanding of the physical phenomena regarding ultrasonic inspection as well as the mechanisms than can lead to the pipe failure and current inspection technologies. Thus, this chapter discusses the essential theoretical background of the propagation of ultrasonic guided waves below the frequency cutoff of high order modes in large diameter pipes. Failure mechanisms observed in water pipes in Northern America are detailed. Finally, current inspection tools are presented and discussed.

1.1 Fundamentals of Ultrasonic Wave Propagation

This study is based on the use of the fundamental principle of mechanical stress wave propagation in a medium. It is then essential to detail equations behind this propagation as well as the associated physical phenomena.

Ultrasound comprises various kinds of mechanical stress waves for which the frequency is above 20kHz (audible limit). It was studied for many years and very detailed books exist on the topic (Cheeke, 2012; Rose, 2014; Royer & Dieulesaint, 1996), presenting the history of this technology as well as a deep explanation of physics behind the propagation of waves in different situations and propagation medium.

1.1.1 Mechanical Bulk Waves Propagation in Solids

Wave propagation was first theorized by d'Alembert for the one-dimensional case and later generalized to any three-dimensional case by Euler. The one-dimensional case highlights essential parameters related to wave propagation such as the wavelength, wavenumber, period

and angular frequency. The three-dimensional generalization brings an understanding of different modes of propagation that can be observed in the propagation of bulk waves.

1.1.1.1 1D Formulation

The general wave motion is described by the d'Alembert formula, also known as the plane wave equation in one dimension:

$$\frac{\partial^2 u(x,t)}{\partial x^2} = \frac{1}{V^2}\frac{\partial^2 u(x,t)}{\partial t^2} \tag{1.1}$$

where V is the constant wave velocity.

The general solution has the form of:

$$u(x,t) = f(x - V.t) + g(x + V.t) \tag{1.2}$$

or

$$\mathrm{U}(x,t) = F\left(t - \frac{x}{V}\right) + G\left(t + \frac{x}{V}\right) \tag{1.3}$$

where f, g, F and G are arbitrary functions and the first term accounts for a propagation in the positive direction along the x axis whereas the second term accounts for the propagation in the negative direction along the x axis.

Considering a sinusoidal perturbation, the solution can now be written as:

$$u(x,t) = A\cos(\omega.t - k.x) \tag{1.4}$$

with:

- $\omega = \frac{2\pi}{T}$ the angular frequency of period T
- $k = \frac{\omega}{T} = \frac{2\pi}{\lambda_{wl}}$ the wavenumber and λ_{wl} the wavelength

Finally, $-k.x$ represents the phase shift and $\Phi_s = \omega.t - k.x$ is the general phase of the wave. The wavenumber k represents the variation of phase Φ_s with position x at a given time t whereas the angular frequency ω represents the variation of phase Φ_s with time t at a given position x.

1.1.1.2 3D Formulation

The wave propagation equation in three dimensions can be obtained from general conservation equations,

$$\rho \frac{\partial^2 u_i}{\partial t^2} = \frac{\partial T_{ij}}{\partial x_j} \tag{1.5}$$

where T_{ij}, the stress tensor for an isotropic solid material, is defined by a generalisation of the Hooke's law:

$$T_{ij} = c_{ijkl} S_{kl}. \tag{1.6}$$

with c_{ijkl} the elasticity tensor and S_{kl} the strain tensor. T_{ij} can also be decomposed and written as

$$T_{ij} = \lambda S_{ii} \delta_{ij} + 2\mu S_{ij} \tag{1.7}$$

where λ and μ are the Lamé parameters we can define using Young's modulus and Poisson's ratio or elasticity tensor of the material:

$$\begin{cases} E = \mu \frac{3\lambda + 2\mu}{\lambda + \mu} \\ \nu = \frac{\lambda}{2\,(\lambda + \mu)} \\ c_{44} = \frac{c_{11} - c_{12}}{2} = \mu \\ c_{12} = \lambda \end{cases}. \tag{1.8}$$

Using equation (1.8) in equation (1.7) we have

$$T_{ij} = c_{12} S_{ii} \delta_{ij} + 2c_{44} S_{ij} = (c_{11} - 2c_{44}) \frac{\partial u_i}{\partial x_i} \delta_{ij} + c_{44} \left(\frac{\partial u_i}{\partial x_j} + \frac{\partial u_j}{\partial x_i} \right). \tag{1.9}$$

Finally, using equation (1.9) in equation (1.5):

$$\rho \frac{\partial^2 u_i}{\partial t^2} = \frac{\partial}{\partial x_i} \left[(c_{11} - c_{44}) \frac{\partial u_j}{\partial x_i} \right] + c_{44} \frac{\partial^2 u_i}{\partial^2 x_j}. \tag{1.10}$$

This equation can be written in its vectorial form

$$\rho \frac{\partial^2 \vec{u}}{\partial t^2} = (c_{11} - c_{44}) \vec{\nabla} (\vec{\nabla} \cdot \vec{u}) + c_{44} \, \Delta \vec{u} \, . \tag{1.11}$$

The three components of the displacement field $\vec{u}$ can be uncoupled using the Helmholtz decomposition theorem and by defining a scalar potential Φ and a vector potential Ψ :

$$\vec{u} = \vec{\nabla} \Phi + \vec{\nabla} \times \Psi = \vec{u}_L + \vec{u}_T \tag{1.12}$$

where $\vec{u}_L$ is a zero curl vector and $\vec{u}_T$ a zero divergence vector.

Thus, using equation (1.12) in equation (1.11) we have two independent equations:

$$V_L^2 \Delta\Phi - \frac{\partial^2 \Phi}{\partial t^2} = 0 \tag{1.13}$$

which corresponds to a pure longitudinal motion depending on the scalar potential Φ and

$$V_T^2 \Delta\Psi - \frac{\partial^2 \Psi}{\partial t^2} = 0 \tag{1.14}$$

which corresponds to a pure shear motion depending on the vector potential Ψ. Each motion is also characterized by a specific wave velocity: V_L for longitudinal wave velocity and V_T for shear wave velocity. The velocities are directly related to the material properties:

$$V_L = \sqrt{\frac{c_{11}}{\rho}} = \sqrt{\frac{\lambda + 2\mu}{\rho}}, \tag{1.15}$$

$$V_T = \sqrt{\frac{c_{44}}{\rho}} = \sqrt{\frac{\mu}{\rho}}. \tag{1.16}$$

The demonstration shows the independent propagation of only two waves types in an isotropic and unbounded solid medium: longitudinal waves (or L-waves or P-waves, meaning pressure waves) and shear waves (or S-waves or transverse waves). Any other wave propagation mode in a solid medium is derived from these two modes of propagation. Figure 1.1 illustrates the deformation induced in a solid medium for both cases. Longitudinal waves propagate thanks to successive compressions and dilatations of a local given material volume (Figure 1.1 a.) and shear waves propagate thanks to the isochoric sliding of parallel and adjacent planes. Depending on the polarization of the wave, we can distinguish shear-vertical waves (or SV-waves) as shown in Figure 1.1 b., where the propagation direction of the wave is along the x-axis and the perturbation (or strain) along z-axis and shear-horizontal waves (or SH-waves), where the propagation direction would still be along the x-axis but the perturbation along y-axis.

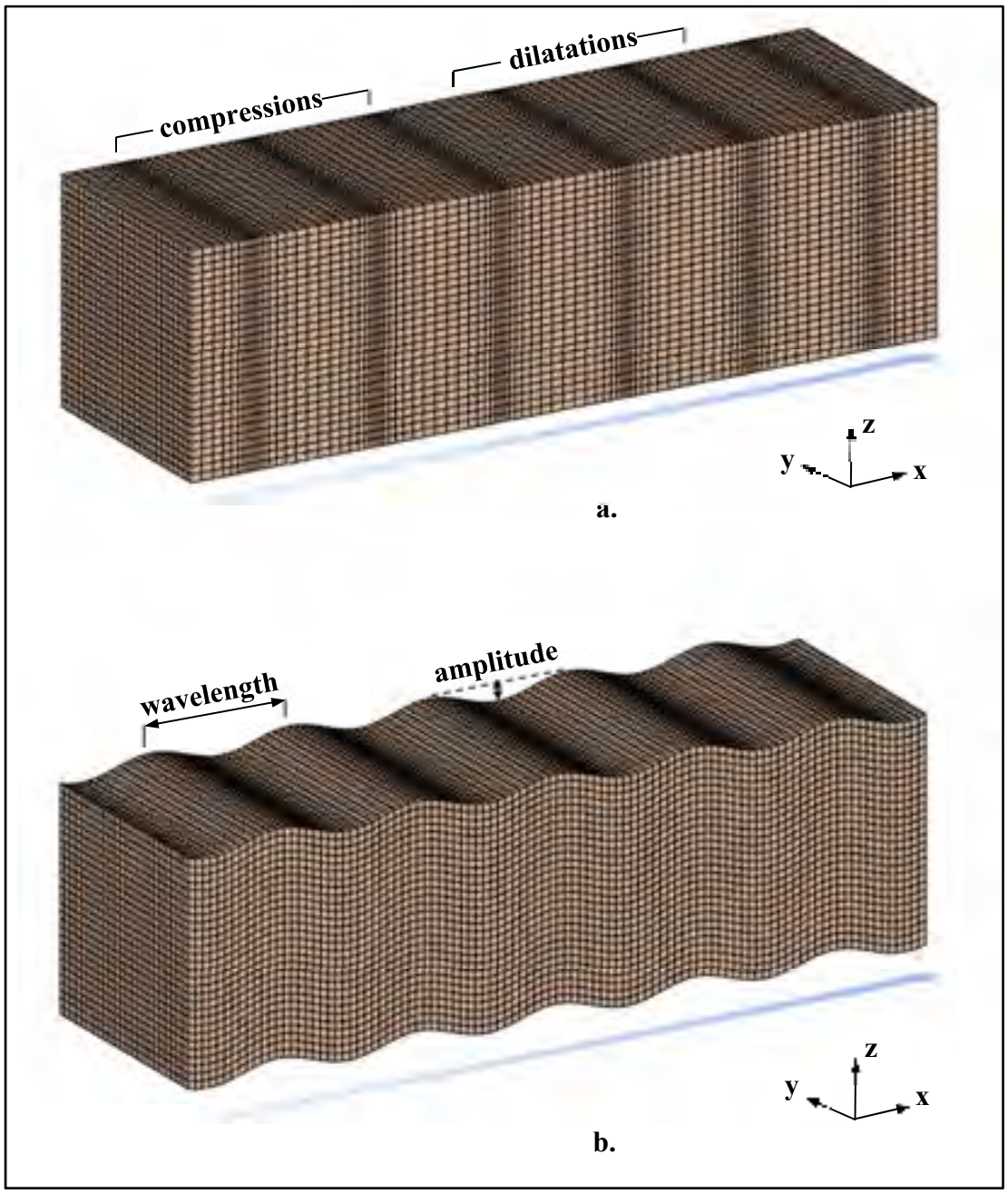

Figure 1.1 Deformation induced in a solid medium by the propagation along the x-axis. a. a longitudinal bulk wave (or P-wave or L-wave) and b. a shear bulk wave (or S-wave or transverse wave)

1.1.1.3 Interactions at boundaries

When a mechanical wave hits a boundary between two isotropic media, a fraction of the incident energy is reflected, and the rest is transmitted. Depending on the mediums and the angle of the incident wave, Snell-Descartes law, or law of refraction governs the resulting mechanical waves.

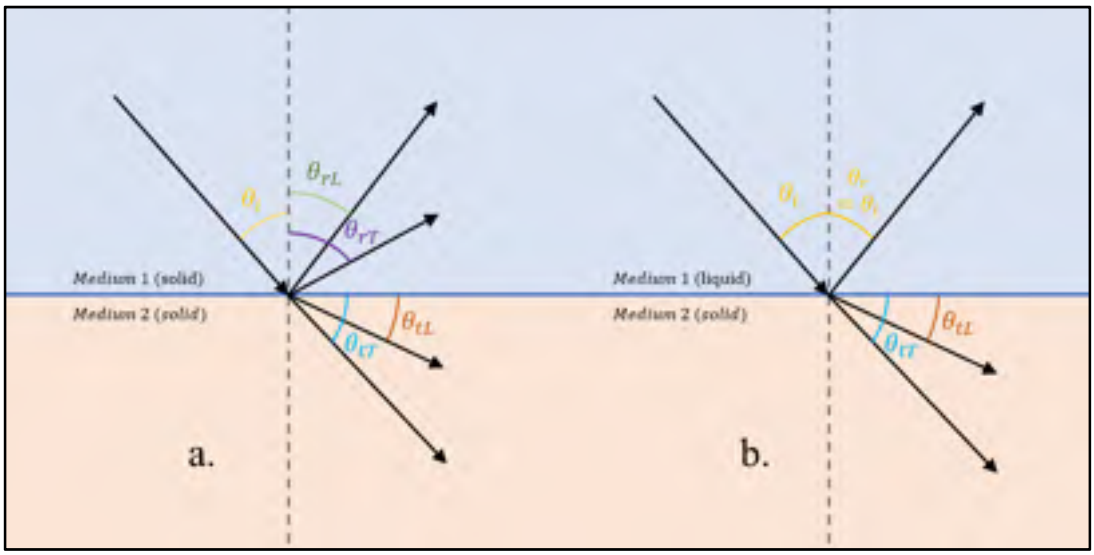

Figure 1.2 Interactions of an incident mechanical wave at a. a solid/solid interface and b. a liquid (non-viscous)/solid interface

Thus, considering the oblique incident wave from a solid medium as represented in Figure 1.2 a., Snell-Descartes law can be expressed:

$$\frac{\sin\theta_i}{V_i} = \frac{\sin\theta_{tL}}{V_{tL}} = \frac{\sin\theta_{tT}}{V_{tT}} \tag{1.17}$$

where θ_i is the incident wave angle, θ_{tL} the angle of the longitudinal transmitted wave and θ_{tT} the angle of the transverse transmitted wave (also called refraction angles) with respective velocities V_i, V_{tL} and V_{tT}. The same rule applies for reflected wave. When the incident medium is a non-viscous liquid as illustrated in Figure 1.2 b., there is only a longitudinal wave reflected with the same angle as incident wave and Snell-Descartes law applies for the second medium.

Additionally, in the case of a normal incidence, the fraction of the reflected and transmitted energy can easily be calculated from the acoustic impedance of both media and are expressed through reflection (R) and transmission (T) coefficients as follows:

$$R = \frac{Z_2 - Z_1}{Z_2 + Z_1} \qquad T = \sqrt{1 - R^2} \tag{1.18}$$

where $Z_n = \rho_n V_n$ is the acoustic impedance of the medium for the designated type of wave.

1.1.1.4 Attenuation

Attenuation is a phenomenon associated to the loss of wave energy with increasing propagation distance in a specific medium. It can be expressed as follows:

$$A(x) = A_0 . e^{-\alpha x} \tag{1.19}$$

with A_0 the initial wave amplitude, A the wave amplitude at a distance x and α the attenuation coefficient. The attenuation coefficient is affected by numerous phenomena such as diffraction, scattering and absorption that lead to energy loss during the propagation of the wave but also by material and excitation properties. It is nevertheless important to remember that attenuation will usually be greater with increasing frequency. Very detailed explanation of the influence of each parameter on the attenuation can be found in reference books (Cheeke, 2012; Dieulesaint & Royer, 1980).

1.1.2 Guided Waves Propagation in Solid Plate-Like Structures

General equations governing the propagation of a bulk wave in a solid medium were established considering an unbounded structure. When the propagation of the wave occurs between the boundaries of a plate or pipe-like structure, specific modes of propagation can appear: ultrasonic guided wave modes. In order to characterize this phenomenon, the propagation of a wave between traction-free surfaces spaced by the finite thickness of a plate (or pipe) like structure is considered. The solution to this problem can be obtained by two techniques than have been well documented in the past: the potential method (Lamb, 1917)

and the partial wave superposition (Solie & Auld, 1973). These methods lead to the plate or pipe ultrasonic guided wave equations described in this chapter.

Two plate guided wave type will be described in this section as they will be useful for the study. Other modes, such as surface Rayleigh waves or Love guided waves in substrates are well documented in books (Cheeke, 2012; Rose, 2014) that give an exhaustive insight on the associated phenomena.

It is also important to note that curves plotted as examples in sections 1.1.2 and 1.1.3 correspond to the structure that will be considered in the simulations part of the study.

1.1.2.1 Shear-Horizontal Waves

Shear-Horizontal waves is the simplest case for ultrasonic guided waves in plate-like structures because of the single horizontal polarization of the wave and its decoupled behavior from other sagittal modes so that there is no mode conversion. As shown in Figure 1.3, assuming a wave propagation in a plate of thickness $2b$ and along the positive direction x, the free surfaces at $y = b$ and $y = -b$ are responsible for the successive reflections of the shear bulk wave with an alternating perturbation parallel to the boundaries along z.

To establish the equations governing the propagation of SH-waves, the use of potential method is simple and well suitable for isotropic media (Rose, 2014). The wave is propagating in the x-direction so that the harmonic solution of equation (1.14) has the form

$$\Psi = \Psi_0(y)e^{i(k_x x - \omega t)}. \tag{1.20}$$

This solution represents a traveling wave in positive x-direction with dependency to time t and a standing wave across thickness (y-axis). Substituting this solution into (1.14) yields an equation governing the unknown potential Ψ. This solution is

$$\Psi_0(y) = A\sin(k_y y) + B\cos(k_y y) \tag{1.21}$$

where

$$k_y^2 = k_s^2 - k_x^2 - k_z^2. \tag{1.22}$$

Since the propagation is in x-direction, k_x represents the wavenumber of SH ultrasonic guided mode, $k_s = \frac{\omega}{V_T}$ represents the bulk shear wavenumber, k_y is related to the wave propagating in the thickness and finally, k_z is equal to zero since there is no wave propagation along z-axis. Using the boundary conditions, strain-displacement relations and Hooke's law, it can be demonstrated (Rose, 2014) that k_y must take discrete value and be equal to

$$k_y = \frac{m\pi}{2b}, \quad m \in \mathbb{N}. \tag{1.23}$$

Using this result in equation 1.17 leads to the SH guided wave dispersion relation:

$$k_x^2 = \left(\frac{\omega}{V_T}\right)^2 - \left(\frac{m\pi}{2b}\right)^2 = \left(\frac{\omega}{V_{\phi_{SH_m}}}\right)^2 = k_{SH}^2 \tag{1.24}$$

where $V_{\phi_{SH_m}}$ is the phase velocity of the SH guided wave mode of order m for the angular frequency ω. After some manipulations it can be rewritten in the form of

$$V_{\phi_{SH_m}} = \frac{V_T}{\sqrt{1 - \left(\frac{m\pi}{2b}\right)^2 \left(\frac{V_T}{\omega}\right)^2}}, m \in \mathbb{N}. \tag{1.25}$$

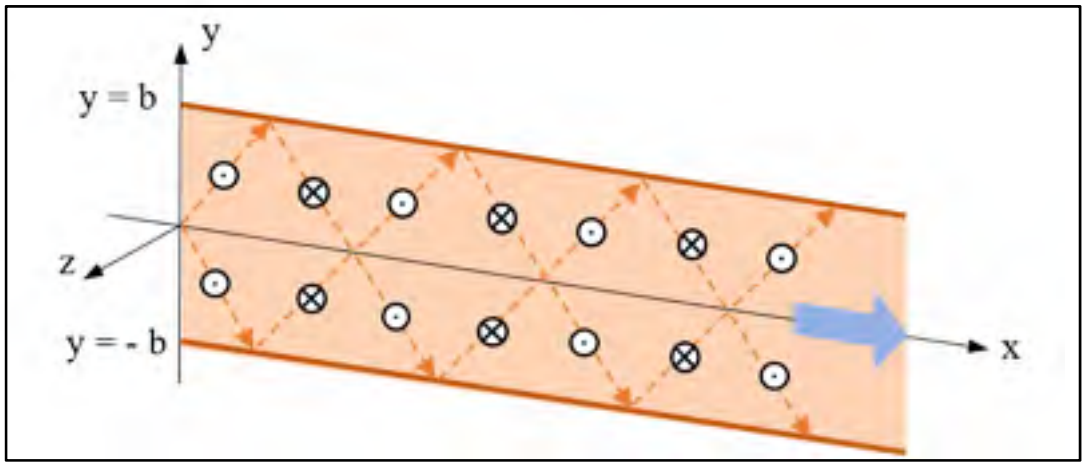

Figure 1.3 Propagation of a Shear-Horizontal (SH) guided wave along x between two free surfaces at $y = b$ and y = $-b$

The phase velocity corresponds to the velocity an observer should move at to see, at any time, the vibration at the same phase state (i.e. $\Phi = \text{constant}$), the wave would then appear as a standing wave.

According to equation (1.24) it can be noticed that, unlike any non-zero order mode for which the velocity is a function of angular frequency ω, the zeroth order mode SH_0 has a constant phase velocity equal to the shear bulk velocity. Thereby it is considered as the only non-dispersive ultrasonic guided wave mode. In case of non-zero values of m, modes can only propagate above a certain frequency so as to keep a real denominator in equation (1.24). Below this cutoff frequency, modes are considered as evanescent. Phase velocity dispersion curves of SH modes can be plotted against the frequency, as shown in Figure 1.4. The cutoff frequency appears clearly for each non-zero order mode as well as the non-dispersive behavior of SH_0.

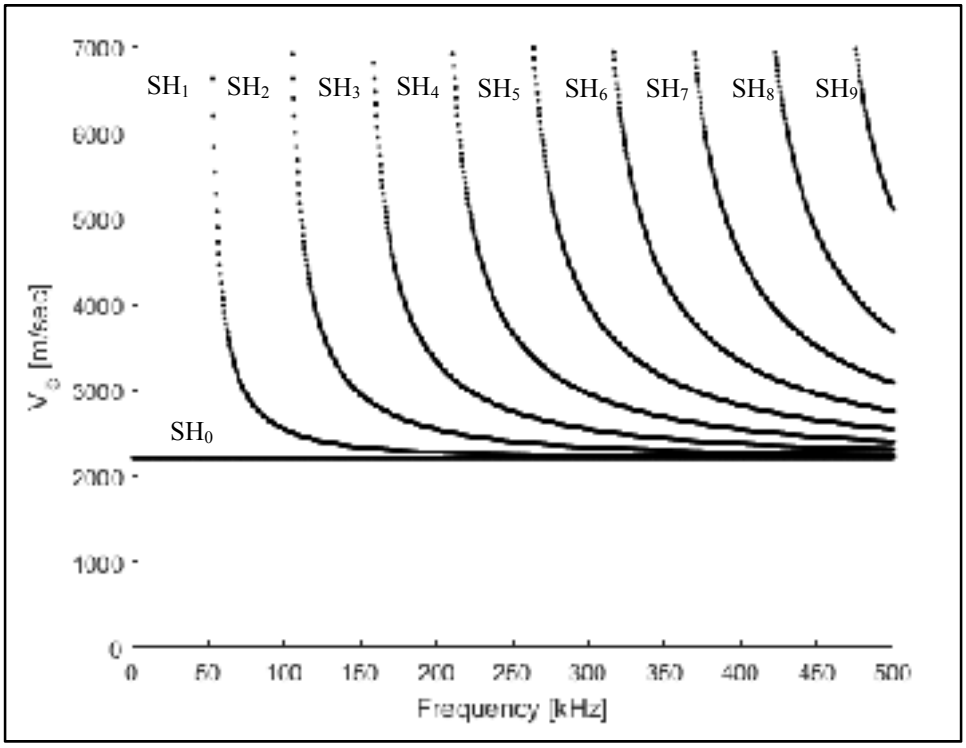

Figure 1.4 Phase velocity dispersion curves of SH modes in a 22 mm thick cast-iron plate (E = 78.3 GPa, ν = 0.17, ρ = 6900 kg/m^3), frequency range is 0-5MHz. Computed using the GUIGUW software (Bocchini, Marzani, & Viola, 2011)

The group velocity of SH guided wave modes which corresponds to the velocity of the wave packet or its energy, is given by the derivative of the angular frequency with respect to wavenumber k,

$$V_{g_{SH_m}} = \frac{d\omega}{dk} = \frac{V_T^2\, k_{SH}}{\omega} = \frac{V_T^2}{V_{\phi_{SH_m}}} \quad , m \in \mathbb{N}. \tag{1.26}$$

Figure 1.5 shows the group velocity dispersion curves for the same frequency range and medium as Figure 1.4 and are rationally inversely proportional to phase velocity curves.

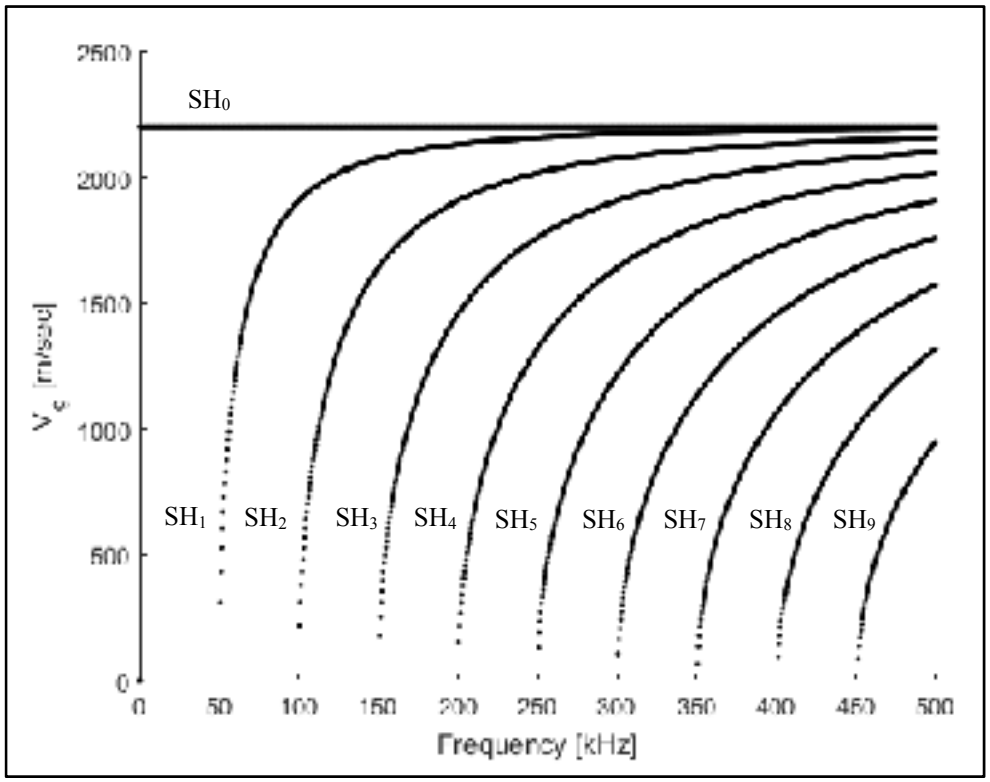

Figure 1.5 Group velocity dispersion curves of SH modes in a 22 mm thick cast-iron plate (E = 78.3 GPa, ν = 0.17, ρ = 6900 kg/m3), frequency range is 0-5MHz. Computed using the GUIGUW software (Bocchini et al., 2011)

1.1.2.2 Lamb Waves

Lamb waves are a more complex case of the propagation of ultrasonic guided waves in plate-like structure. Indeed, they correspond to the solution of the free plate problem related to the propagation of two type of waves in the sagittal plane: longitudinal waves and shear-vertical waves. Both waves are coupled and result from successive reflections, where mode conversion occurs, at the surface of the structure as illustrated in Figure 1.6. The full demonstration of

Rayleigh-Lamb wave equations that describe the propagation of Lamb wave modes will not be expressed as many textbooks (Auld, 1973; Cheeke, 2012; Lamb, 1917) give very detailed procedure using both the partial wave or potential methods. To satisfy the free plate problem with free surfaces at $y = b$ and $y = -b$, both longitudinal and shear-vertical waves must share the same wavevector component in propagation along the x direction. This condition can be written, using the previously introduced equation (1.22) :

$$\begin{cases} k_{y,L}^2 = k_L^2 - k_x^2 - k_z^2 = \left(\frac{\omega}{V_L}\right)^2 - k_x^2 \\ k_{y,S}^2 = k_s^2 - k_x^2 - k_z^2 = \left(\frac{\omega}{V_T}\right)^2 - k_x^2 \end{cases} \tag{1.27}$$

where k_x is the common wavevector component in propagation direction x and $k_{y,L}$, $k_{y,S}$ are wavevector components normal to the plate surface of respectively L-wave and SV-wave. Finally, applying conservation equations and after some algebra, the Rayleigh-Lamb frequency equations are

$$\frac{\tan(k_{y,S}\, b)}{\tan(k_{y,L} b)} = -\frac{4\, k_x^2\ k_{y,L}\, k_{y,S}}{\left(k_{y,S}^2 - k_x^2\right)^2} \tag{1.28}$$

for symmetric solutions and

$$\frac{\tan(k_{y,S}\, b)}{\tan(k_{y,L} b)} = -\frac{\left(k_{y,S}^2 - k_x^2\right)^2}{4\, k_x^2\ k_{y,L}\, k_{y,S}} \tag{1.29}$$

for antisymmetric solutions. These solutions are directly related to symmetric (S_m) and antisymmetric (A_m) modes that are usually represented by dispersion curves of both phase and group velocities as shown in Figure 1.7 and Figure 1.8. Dispersion relationships can be obtained by substituting (1.27) into (1.28) and (1.29) but due to their transcendental characteristic they have to be solved numerically, for example, using DISPERSE (Pavlakovic, Lowe, Alleyne, & Cawley, 1997), or by a semi analytical finite-element (SAFE) method which is not subjected to numerical instabilities, for example, using GUIGUW (Bocchini et al., 2011). It can be observed that, unlike SH modes, all Lamb modes are dispersive and the high order modes characterized by a cutoff frequency. Additionally, the number of modes is increasing with frequency and it exists some frequency regions where modes can be considered as virtually non-dispersive.

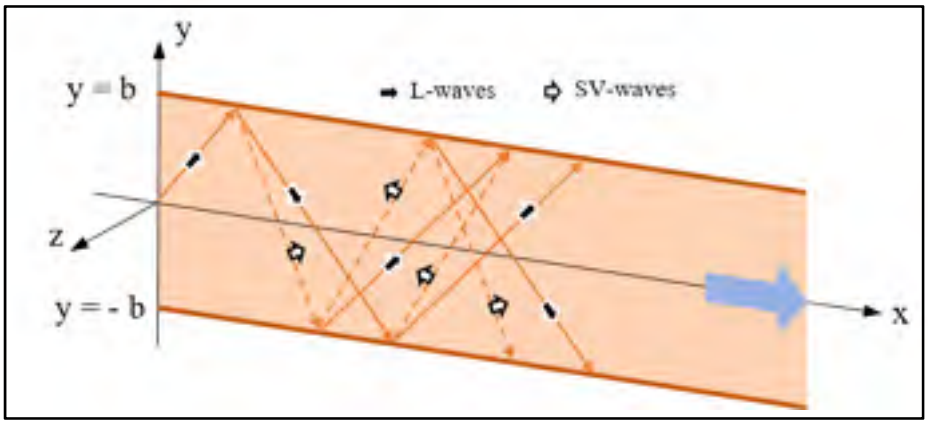

Figure 1.6 Propagation of Lamb guided waves along x between two free surfaces at $y = b$ and $y = -b$. Mode conversion (L-waves and SV-waves) occurs at each reflection on the surface

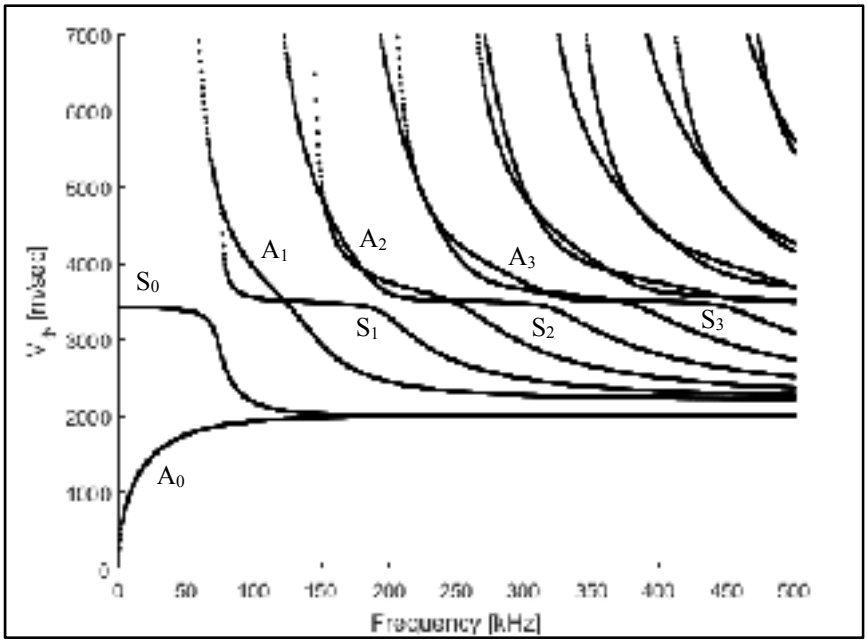

Figure 1.7 Phase velocity dispersion curves of Lamb modes in a 22 mm thick cast-iron plate (E = 78.3 GPa, ν = 0.17, ρ = 6900 kg/m3), frequency range is 0-500kHz. Computed using the GUIGUW software (Bocchini et al., 2011)

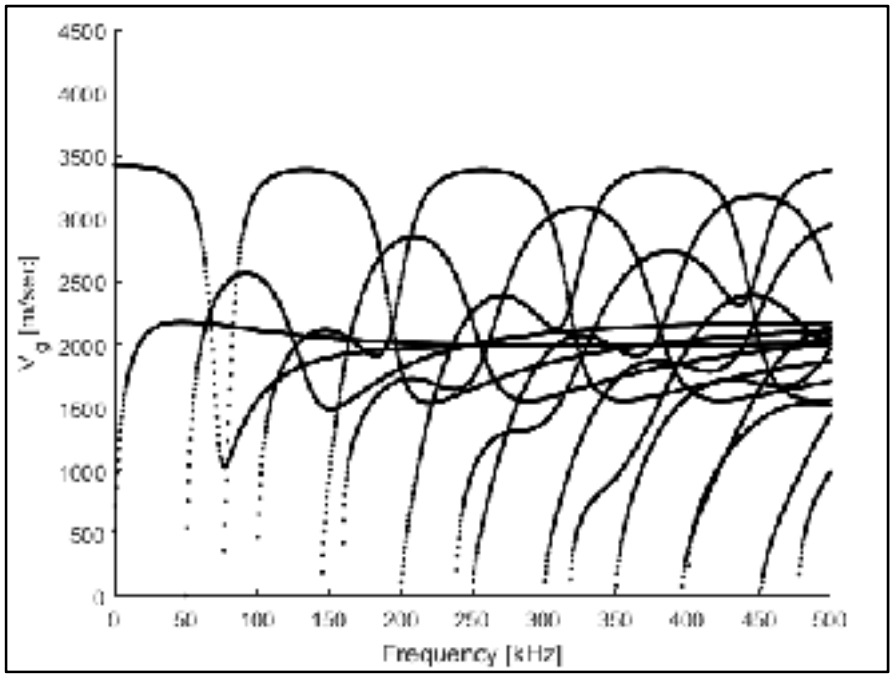

Figure 1.8 Group velocity dispersion curves of Lamb modes in a 22 mm thick cast-iron plate (E = 78.3 GPa, ν = 0.17, ρ = 6900 kg/m3), frequency range is 0-500kHz. Computed using the GUIGUW software (Bocchini et al., 2011)

1.1.3 Guided Waves Propagation in Solid Pipe Structures

Pipe guided wave modes are close to plate ones. Hence, modes similar to Lamb and SH modes exist as well as specific modes such as flexural pipe modes. The plate analogy highly depends on the ratio of the pipe diameter to the pipe thickness. This section will briefly introduce the different pipe guided waves modes. As the method to find propagation equation solutions, based on potential functions, is close to the one of free-plate case, it will not be described but is well documented in a variety of textbooks (Cheeke, 2012; Rose, 2014).

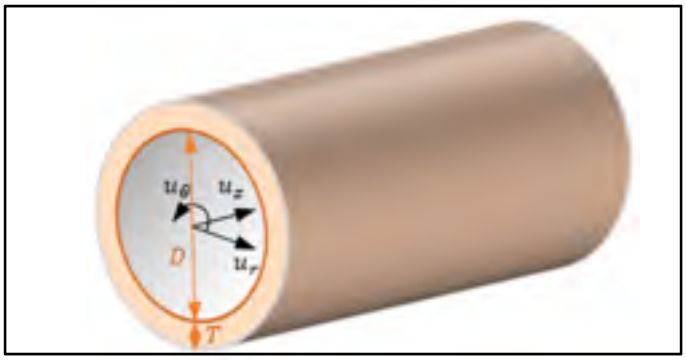

Figure 1.9 Cylindrical coordinate set and pipe geometry

1.1.3.1 Torsional Pipe Modes

Torsional pipe modes are similar to shear-horizontal modes in plate-like structures. Using cylindrical coordinates as shown in Figure 1.9, displacement is only induced on u_θ so as to create a shear motion. Phase velocity dispersion curves of pipe torsional modes can be plotted using the same software and for the same material in a 22 mm thick pipe of diameter 309 mm as shown in Figure 1.10. Dispersion curves are identical to the ones plotted for the free-plate case except for the numbering of modes $T(0, m)$ where m refers to the mode number and zero refers to the circumferential order, which, in this case means that this type of mode is axisymmetric.

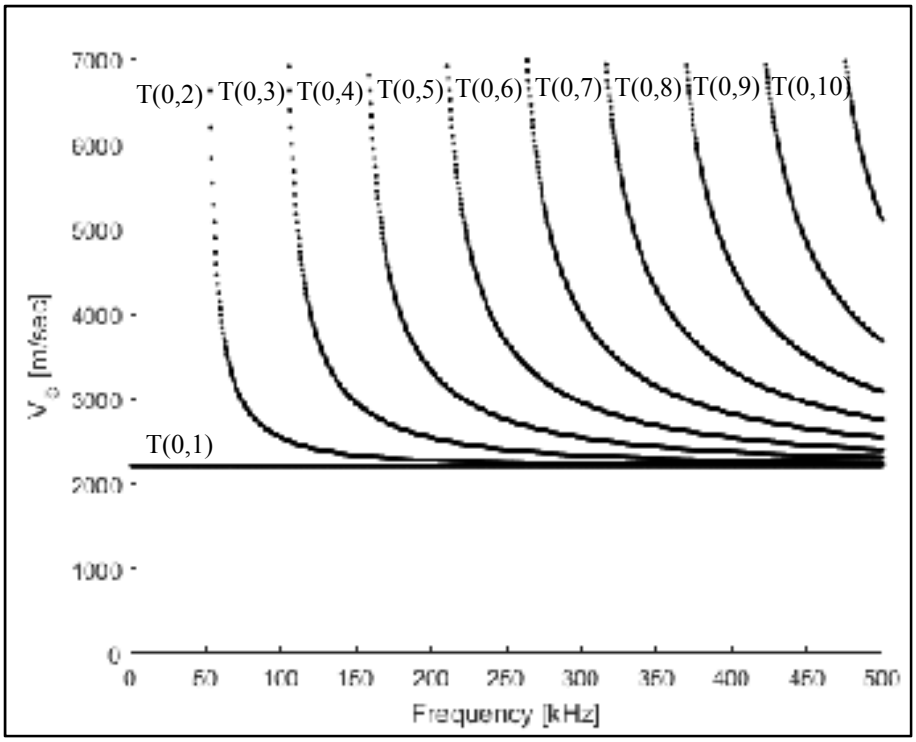

Figure 1.10 Phase velocity dispersion curves of pipe torsional modes in a 22 mm thick cast-iron pipe of diameter 309 mm (E = 78.3 GPa, ν = 0.17, ρ = 6900 kg/m3), frequency range is 0-500kHz. Computed using the GUIGUW software (Bocchini et al., 2011)

1.1.3.2 Longitudinal Pipe Modes

Longitudinal pipe modes are similar to Lamb modes in plate-like structures. Using cylindrical coordinates as shown in Figure 1.9, displacement is only induced along u_z and u_r so as to create a compression and a shear motion. Phase velocity dispersion curves of pipe longitudinal modes can be plotted using the same software and for the same material in a 22 mm thick pipe of diameter 309 mm as shown in Figure 1.11. Dispersion curves are quasi-identical to the ones plotted for the free-plate case except for very low frequencies where there are deviations. Longitudinal modes are numbered L(0,m) where m refers to the mode number and zero refers to the circumferential order, which, in this case means that this type of mode is also axisymmetric.

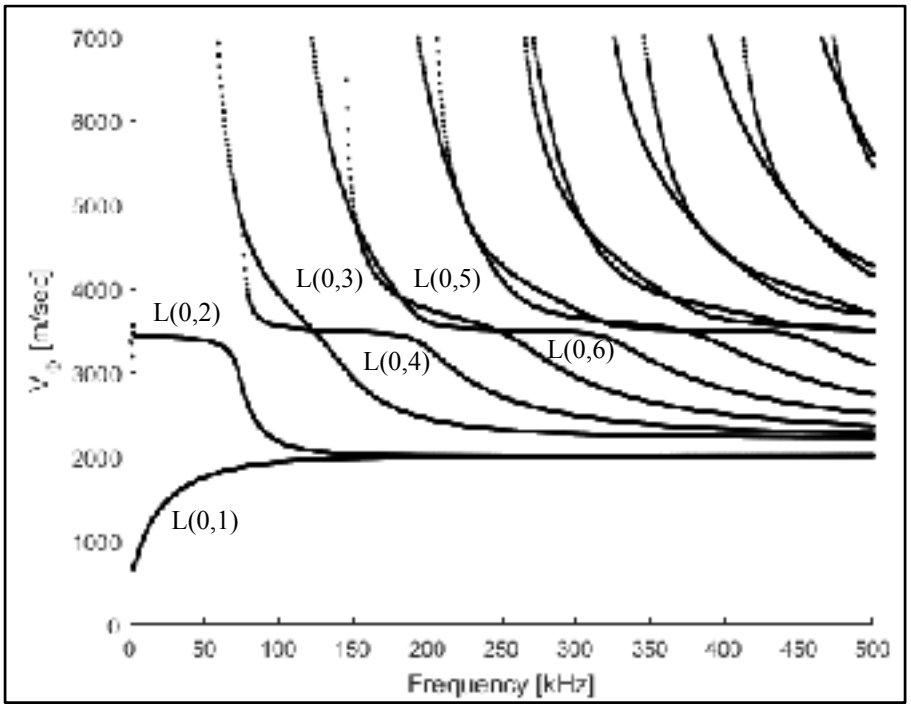

Figure 1.11 Phase velocity dispersion curves of pipe longitudinal modes in a 22 mm thick cast-iron pipe of diameter 309 mm (E = 78.3 GPa, ν = 0.17, ρ = 6900 kg/m3), frequency range is 0-500kHz. Computed using the GUIGUW software (Bocchini et al., 2011)

1.1.3.3 Flexural Pipe Modes

In opposition to torsional and longitudinal pipe modes, flexural pipe modes have a circumferential order depending on angle θ and are consequently non-axisymmetric. Displacements exist along all directions u_r, u_θ and u_z. If flexural modes are clearly identifiable at a low frequency and for a low diameter to thickness ratio they quickly convert to either longitudinal or torsional modes at higher frequencies and thickness to diameter ratios as illustrated in Figure 1.12. Phase velocity dispersion curves are represented up to the 5th order for a diameter to thickness ratio of 8 and for a low frequency range from 0 to 100 kHz.

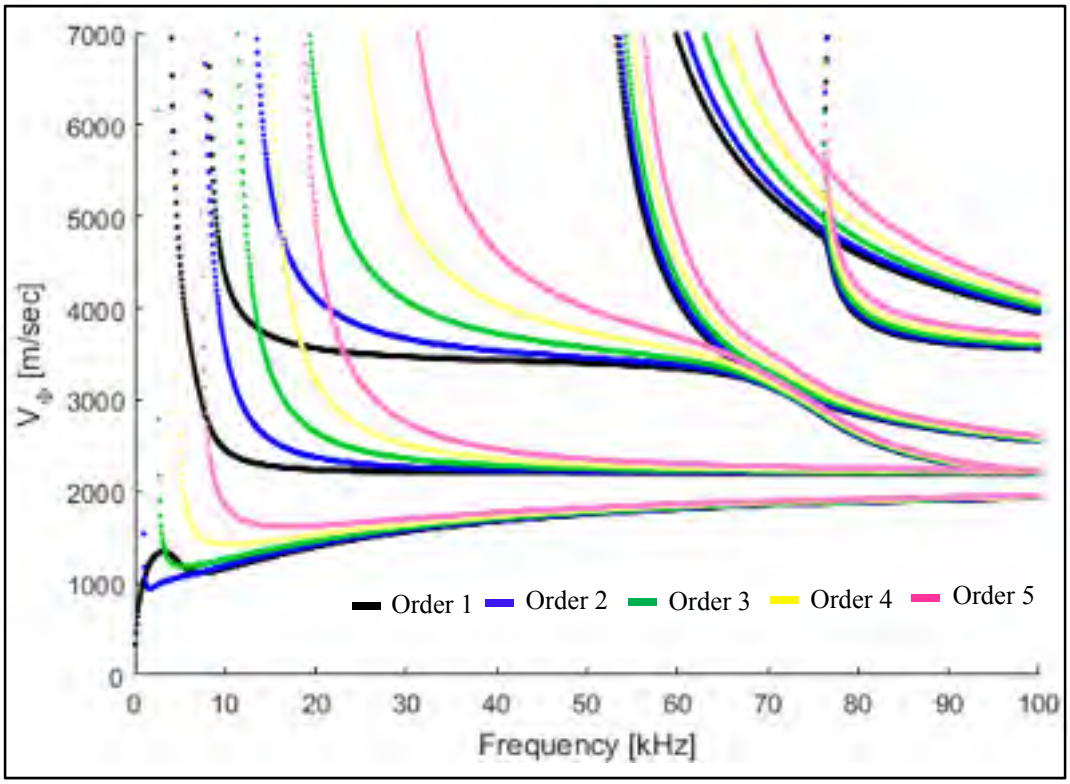

Figure 1.12 Phase velocity dispersion curves of pipe flexural modes (order 1 to 5) in a 22 mm thick cast-iron pipe of diameter 88 mm (E = 78.3 GPa, ν = 0.17, ρ = 6900 kg/m3), frequency range is 0-100kHz. Computed using the GUIGUW software (Bocchini et al., 2011)

1.1.3.4 Plate Analogy

As introduced in previous sections and developed by (Li & Rose, 2006), if the diameter to thickness ratio becomes large, pipe modes are quickly similar to Lamb modes with increasing frequency as illustrated in Figure 1.13 where a variable diameter to thickness ratio (D/T) is considered for a 22 mm thick pipe of diameter going from 44 mm to 352 mm and longitudinal phase velocity dispersion curves are plotted. It can be observed that pipe longitudinal modes are getting closer to Lamb modes for a plate of the same thickness at higher frequencies. Thus, a plate analogy can be made when mode behavior in pipes are similar to those in plates and therefore simplify the modelling and experiments. It is possible to define a frequency limit where the plate analogy remains true, using Figure 1.13 it can be assumed that this

approximation is good above a frequency of 50kHz. This limit will shift either to higher or lower frequencies with changing thickness and material properties.

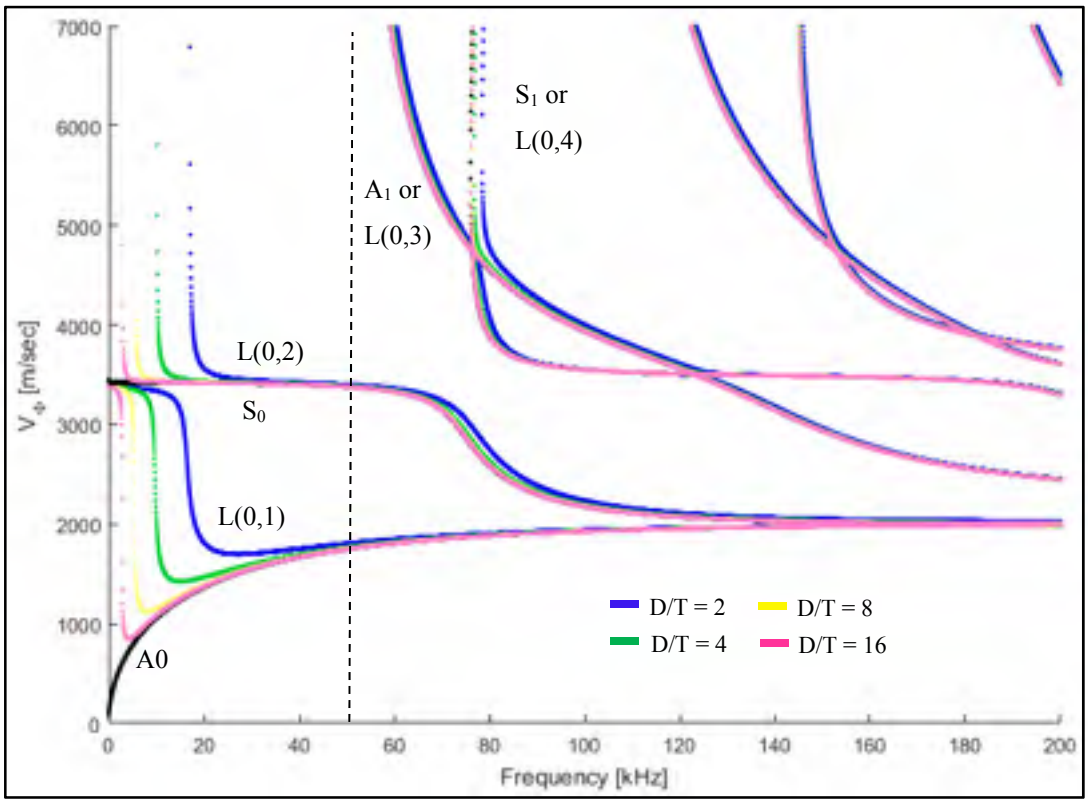

Figure 1.13 Phase velocity dispersion curves of plate lamb modes (black) and pipe longitudinal modes in a 22 mm thick plate and cast-iron pipe respectively of diameter 44 (blue), 88 (green), 176 (yellow) and 352 (pink) mm (E = 78.3 GPa, ν = 0.17, ρ = 6900 kg/m3), frequency range is 0-2MHz. Computed using the GUIGUW software (Bocchini et al., 2011)

1.1.4 Conclusion on Wave Propagation and Ultrasound

Theoretical background of pipe guided waves at a low frequency and in a large diameter pipe was presented from the basics of mechanical wave propagation to a deep explanation of plate guided waves and their analogy in large diameter pipes. This knowledge will be helpful in the following chapters to understand physical phenomena that will be observed and choices that will be made for both simulations and experimental studies.

1.2 Water Pipes Failures

This project aims to improve the current inspection methods of water pipes for Northern American networks. It is then important to know the kinds of failure the inspection tool will have to detect or image and phenomena that usually lead to these failures. Thus, this section will present different failures causes and their modes identified by Canadian (Makar, Desnoyers, & McDonald, 2001) and American (American Water Works Service Co, 2002) water networks authorities, scientists and companies in the last decades. Considering that this project is mainly focused on cast-iron pipes that were predominantly used in the early nineteen hundreds (American Water Works Service Co, 2002) and still represent a significant portion of the currently installed pipes, only failure mechanisms observed for cast-iron will be presented.

1.2.1 Failures Causes of Cast-Iron Water Pipes

Failures of cast-iron water pipes, that lead to crack initiation, have various causes produced mainly by manufacturing, environmental conditions and utilization of the pipe.

1.2.1.1 Manufacturing Process Causes

The manufacturing process of cast-iron pipes, especially in the early nineteen hundreds when water networks were built rapidly is a major source of material weakening. Thus, pit casting was first used, and important porosity was observed due to air trapped during the pouring and solidification phases in the vertical mould. A non-uniform thickness of the pipe was also commonly observed when using this technique. Then, spin or centrifugal casting was used to ensure a more uniform distribution of molten metal in the mould and avoid porosities but undissolved ferrosilicon inclusions, used to lower the melting point, as well as iron oxide on the outer surface was observed (Makar, 2000; Makar et al., 2001). Iron phosphide was also used to lower the melting point but weakens the materiel due to its more important brittle characteristic than cast iron. Finally, it has also been proved that the use of lamellar graphite

iron over a spheroidal graphite iron produces a more important brittleness (Felli & Lupi, 2016) and that spheroids size is also crucial for breakproof (Berdin, Dong, & Prioul, 2001).

1.2.1.2 Environmental Causes

Environmental causes are also of a great importance for the pipe lifespan. The first one is indisputably corrosion which is most of the time the reason of major breaks, thinning of the pipe wall can lead to cracks and holes. This phenomenon is due to the water circulating inside the pipe but also to the surrounding soil which is more or less suitable to the initiation of the reaction depending of its nature (sand, clay, etc.). Then, there is also the forces induced between the soil and the pipe, whether of thermal origin due to the evolution of temperature of the soil and the water according to the seasons or geological due to movements of the ground (Rajani, Zhan, & Kuraoka, 1996). These stresses can lead to premature failure in stress concentration zones, owing to pipe geometry, manufacturing, or caused by corrosion.

1.2.1.3 Utilization and Human Causes

Finally, the use of the pipe itself is harmful to its breaking strength. Thus, hydraulic transients such as pressure variations inherent to the use of the network (Rezaei, Ryan, & Stoianov, 2015) and particularly water hammers generated by sudden closing of a valve or the starting of a high power pump (American Water Works Service Co, 2002) generate shocks and stresses that will undermine the entire structure. Fatigue can therefore appear, however, signs of this phenomenon are rarely observed. It should also be noted that human activity such as construction work could also be harmful to water networks and then lead to failures especially during excavation operations.

1.2.2 Failures Modes of Cast-Iron Water Pipes

After having identified different causes that can lead to a pipe failure this section will present the different failures modes that mainly depend on pipe size and were observed on Northern American water networks.

1.2.2.1 Small Pipes Failure Modes

First, small pipes which diameter is generally under 380 mm are more prone and exposed to many failure modes (Atkinson, Whiter, Smith, & Mulheron, 2002; Makar et al., 2001) than larger pipes as shown on Figure 1.14 :

- Bell splitting (Figure 1.14 c.): generally generated by a difference of thermal expansion coefficient between the pipe and the joint, commonly composed of lead or leadite, at the connection with the male part. This kind of rupture is easily identifiable by a longitudinal separation, a crack, from the bell which then continues circumferentially due to stresses release.
- Corrosion pitting: local thinning of the pipe wall which may lead to through-thickness holes (Figure 1.14 b.) or chain created corrosion (Figure 1.14 e.).
- Axial cracking (Figure 1.14 a.): generally generated by excessive pressure in the pipe or compressive stresses and associated with corrosion bell-initiated crack.
- Circumferential cracking (Figure 1.14 d.): generally generated by bending or tensile stresses and associated with corrosion chain.

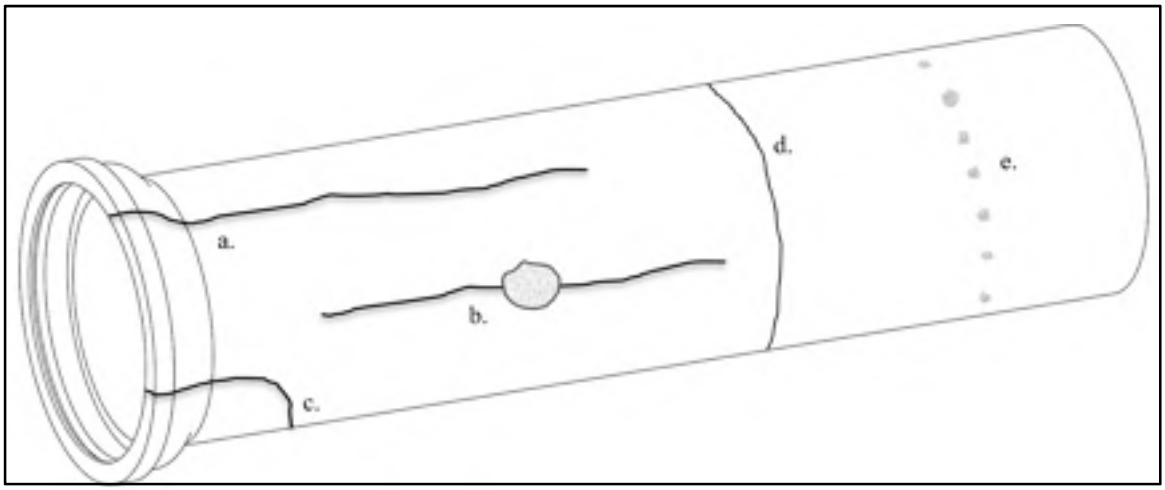

Figure 1.14 Small pipes (diameter < 380mm) failure modes. a. axial crack initiated at the bell, b. axial crack initiated due to corrosion pitting and pipe wall thinning, c. bell splitting, d. circumferential cracking, e. chain created corrosion

1.2.2.2 Large Diameter Pipes Failure Modes

Large diameter pipes are less prone to failures due to their thicker walls, higher moment of inertia and their higher capacity to support important loads. They are nevertheless affected by some particular failures modes as illustrated in Figure 1.15 : Bell shearing (Figure 1.15 a.) and longitudinal splitting (Figure 1.15 b.) which origins are close to small pipe failures modes, and spiral failures (Figure 1.15 c.) which are generally generated by a combination of bending stresses and pressure surges.

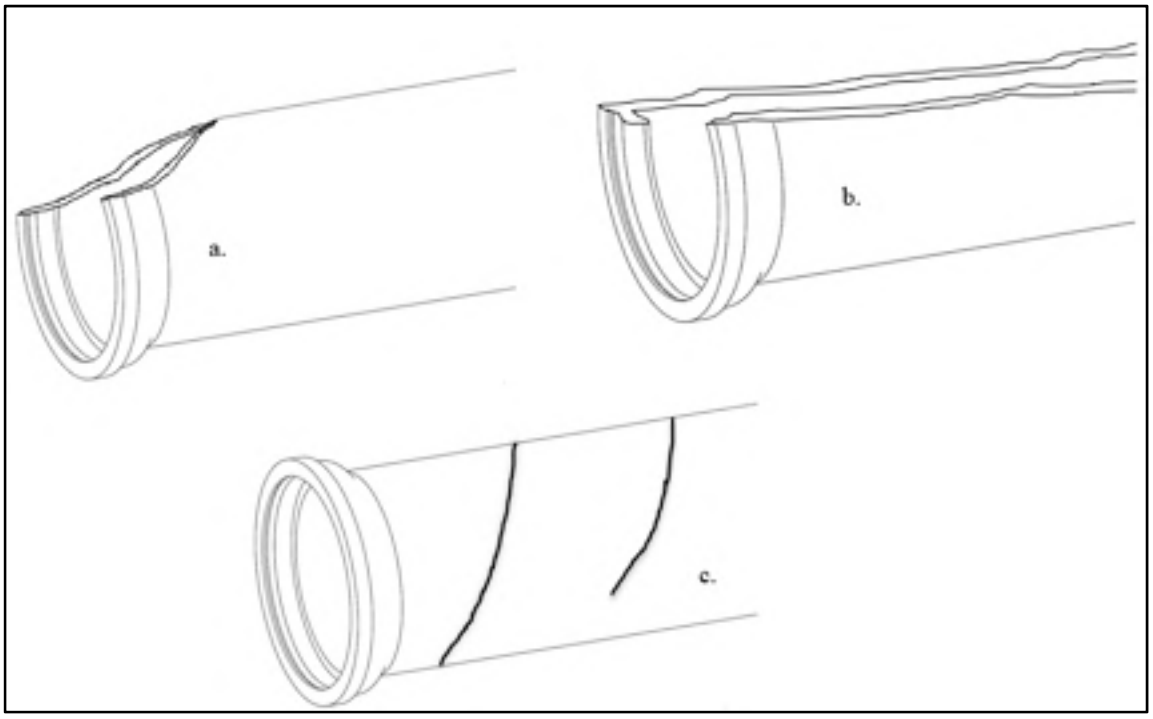

Figure 1.15 Large pipes (diameter > 380mm) failure modes. a. bell shearing, b. longitudinal splitting and c. spiral failures

1.2.3 Conclusion on Water Pipes Failures

Main cast-iron water pipe failures, their causes and their modes were reviewed. Due to the aging characteristic of Northern American water networks, the majority of the information provided took their origin from studies based on observation of many failures. The failure that will be considered for modeling and experimental inspection in the following chapters of this study is the large diameter pipe axial cracks.

1.3 Water Pipes In-Line Inspection Solutions

Various technical solutions exist in order to conduct the in-line inspection, or pigging, of a water pipe and will be briefly introduced in this section. It is however important for the reader to clearly distinguish in-line solutions from solutions requiring the excavation of a pipe section (if buried), such as ultrasonic transducer rings or other guided wave solutions (Cawley, Lowe,

Alleyne, Pavlakovic, & Wilcox, 2003; Leinov, Cawley, & Lowe, 2014) using the outer part of the pipe to conduct the inspection. These solutions are more often used for oil and gas pipelines which are more accessible than water networks. In-line inspection tools for water networks have the advantage of being a wide range solution for a fast inspection of long pipelines.

1.3.1 Magnetic Flux Leakage (MFL)

Magnet flux leakage solutions are among the oldest and most popular (M. Beller, 2002) that are used on in-line inspection devices, or PIG. The principle of this technique is to use the pipe wall as a guide for magnetic flux generated by a permanent magnets or electromagnets. If there is any defect between both the poles of the magnet, the magnetic flux will leak and is measured in three dimensions, that is to say along the axial, circumferential or radial direction, by a sensor placed between these poles. The waveform associated with the magnetic leakage field can then be related to the defect size and shape. This technique is particularly suitable for the detection of pit corrosion, wall thinning and scratches (Huadong et al., 2018). It can operate in difficult environments such as high temperature or cold and under water but remains sensitive to pipe thickness and magnetization conditions.

1.3.2 Ultrasonic Testing

Ultrasonic testing has been well developed over the last years for in-line inspection operations whether with piezoelectric probes or electromagnetic-acoustic transducers (EMAT)

1.3.2.1 Piezoelectric Transducers

Piezoelectric transducers is the most commonly used type of transducer for ultrasonic testing applications. The physical phenomenon behind this technology is basically an electromechanical coupling achieved by a piezoelectric crystal. The crystal is excited by an electrical signal and a mechanical wave proportional to this signal is generated. This is also known as the inverse piezoelectric effect. For the reception of the signal, the inverse

phenomenon is used, called the direct piezoelectric effect. The main challenge when dealing with the inspection of pipes is the coupling between the piezoelectric transducer and the pipe wall. Considering the case of the in-line inspection of a water pipe, it is not a problem since the water is pressurized and can be used as a couplant. It is however more difficult for gas pipelines inspection. Piezoelectric transducers are known for their accurate measurement of the pipe wall thickness and have been used for a long time in addition to MFL solutions for this purpose. They can now achieve more precise measurements such as the detection of axial and circumferential cracks thanks to angled insonification and the use of multiple reflections in the pipe wall thickness (Reber, Beller, Willems, & Barbian, 2002). The principle used is closed to the one used for weld inspection using a wedge. The main drawback of this solution is that it requires a huge number of transducers (up to 300) to cover the entire pipe circumference, which means that the hardware behind will also be very heavy and expensive. In this project, we will use piezoelectric transducers as well but in a different manner, thanks to ultrasonic guided waves, so as to reduce the number of transducers required and the associated cost.

1.3.2.2 EMAT

Electromagnetic-acoustic transducers do not require a couplant to generate an ultrasonic wave in the pipe wall. Indeed, these transducers are made of a magnet (permanent or electromagnetic) and a coil. An exciting current is sent to the coil and induced eddy-currents will then be generated in the conducting pipe wall. These eddy-currents, under the influence of the magnetic field will finally give birth to Lorentz forces (i.e. a stress) allowing the generation of ultrasonic waves at a frequency corresponding to the excitation signal of the coil. The inverse phenomenon is used for reception. Thanks to different magnet/coil arrangements, various modes can be excited (either longitudinal or transverse). Even if it does not require a coupling agent, the main drawback lies in the lift-off allowed between the transducer and the pipe wall which must be kept small and constant. It also requires a high embedded power supply. This technology is however able to detect precisely cracks, thickness loss and many other defects (Feng et al., 2017).

1.3.3 Eddy Current Testing

Eddy-current testing relies on the induction of eddy-current in the pipe wall thanks to coils that are used both for excitation and/or reception. The presence of a defect will change the eddy current flow and can then be measured by the reception coil. This technology is able to detect small cracks and corrosion but is very sensitive to the probe orientation and the lift-off between the probe and the pipe wall as well as the equipment speed in the pipe (Huadong et al., 2018). This technology is sometimes used in combination with EMAT or MFL solutions using shared hardware such as coils and magnets (Willems, Jaskolla, Sickinger, Barbian, & Niese, 2010).

1.3.4 Conclusion on Water Pipes In-Line Inspection Solutions

Most common in-line inspection solutions that can be used for water pipe lines were presented. It is important to note that none of these solutions represent a perfect choice for water pipeline inspection and service company will often equip their PIG with different technologies to compare acquired information. This project will be focused on the development of a simpler solution for ultrasonic testing using piezoelectric probes and the use of ultrasonic guided waves in a close relationship with the partner company involved in this project.

CHAPTER 2

EVALUATING THE INSPECTION METHOD BY FINITE ELEMENT SIMULATIONS

Having now reviewed the knowledge required to conduct the feasibility study of the in-line inspection of large diameter cast-iron water pipes axial cracks using ultrasonic guided waves, this chapter will present the proposed inspection method as well as its assessment through finite element simulations, either in 2D and 3D. The pipe geometry that will be considered is a 24-inch diameter pipe made of grey cast iron, 22mm thick. The large diameter to thickness ratio ($D/T = 28$) allows to use the plate analogy for ultrasonic guided wave modes. The fundamental A_0 plate mode or its equivalent $L(0,1)$ pipe mode will be exploited as it has a strong out-of-plane displacement which can be excited and detected using water as a couplant.

Simulations were conducted using Abaqus® and Pogo FEA. Abaqus® uses Central Processor Units (CPUs) whereas Pogo FEA (Huthwaite, 2014) uses Graphical Processor Units (GPUs) to perform the resolution of equations. The use of GPU allows to parallelize the calculation on much more cores than CPU for an affordable price, resulting in drastic computation time reduction (up to 100 times). It is particularly interesting when dealing with large models such as the one considered for three-dimensional simulations. On both solvers, the explicit scheme was used and simulation parameters such as elements size, time step and time period were carefully selected (M. B. Drozdz, 2008). Simulations were performed in the time domain to simulate the experimental implementation.

2.1 The inspection method

The inspection method that will be modeled will be first introduced through a brief overview of the whole process and a detailed explanation of the measurement method will follow.

2.1.1 Overview of the process

The proposed inspection method consists in the propagation of an ultrasonic guided wave in the pipe wall circumference that will interact with a potential axial crack. The measurement of this interaction as well as the insonification are conducted using ultrasonic piezoelectric transducers located close to the pipe surface and that are equally distributed on a circular array mounted on the PIG as schematized in Figure 2.1.

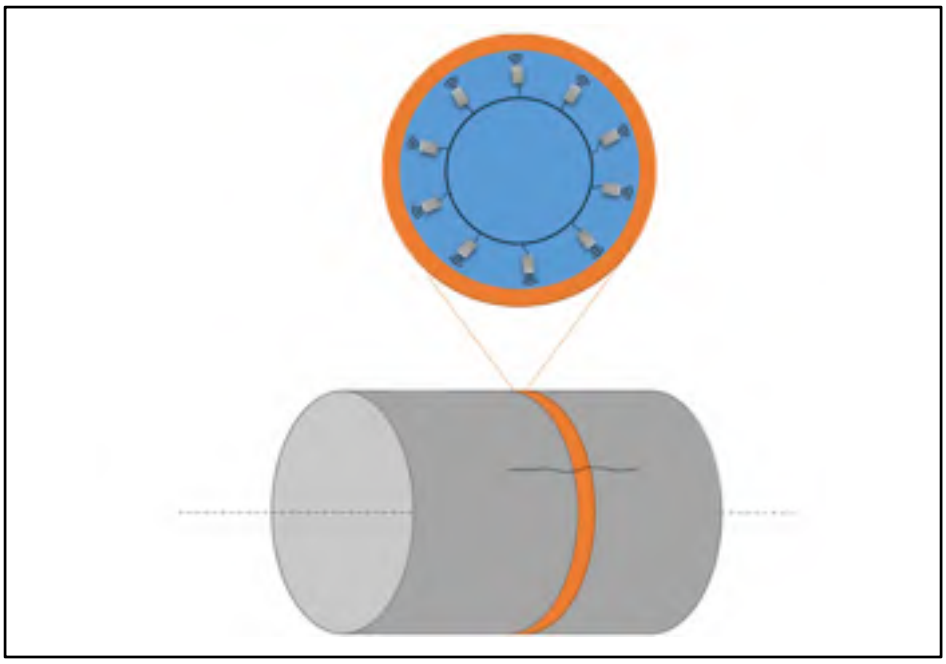

Figure 2.1 Transducers arrangement along a circular array on the PIG

Using the interaction with the axial crack and by knowing propagation velocities in both the water and the pipe wall, an image of the pipe wall integrity can then be generated by exploiting constructive interferences that will result of the summation of the received signals along the pipe circumference for each transducer and for a specific axial range of the pipe. Conducting this measurement continuously while the PIG is moving will lead to an image representing the pipe wall integrity along the inspection range. The full inspection process is represented in Figure 2.2.

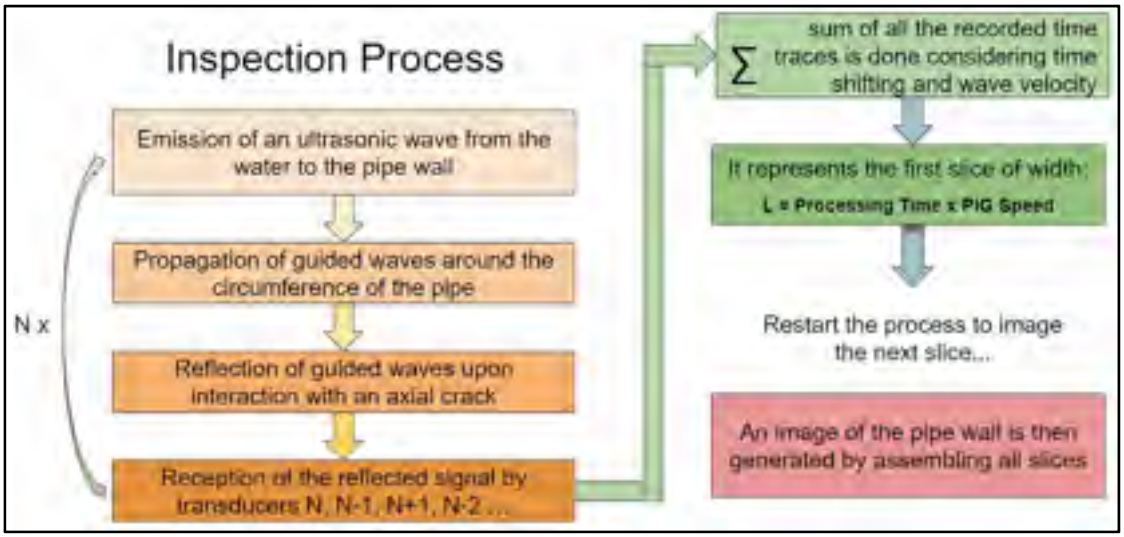

Figure 2.2 Inspection process

2.1.2 Step by step measurement method

To accomplish this measurement and considering the transducers arrangement presented in Figure 2.1, the measurement method can be detailed as follows:

- At a given time t, transducer N (and only transducer N) is fired (Figure 2.3 a.).
- The ultrasonic guided wave propagates through the pipe wall and is received by transducers $N-1$ and $N+1$ (Figure 2.3 b.).
- If the wave is reflected by a crack between transducer N and $N-1$ or between transducer N and $N+1$, transducer N receives the reflected part of the signal and transducer $N-1$ or $N+1$ receives a signal with a lower amplitude compared with the no defect case (Figure 2.3 c.).
- Signals received at transducer $N-1$, N and $N+1$ are compared and analyzed so as to determine the crack position and severity: If the amplitude of the signal received at transducer $N-1$ is lower than the amplitude of the signal received at transducer $N+1$, then it is assumed that the crack is located between N and $N-1$. Time-of-Flight (TOF) between emitted signal from transducer N and reflected signal from crack is used to determine the distance (angular position) of the crack, knowing the wave speed

in the pipe wall. This information will be confirmed when transducer $N-1$ will be fired in turn (so as to create a constructive interference).

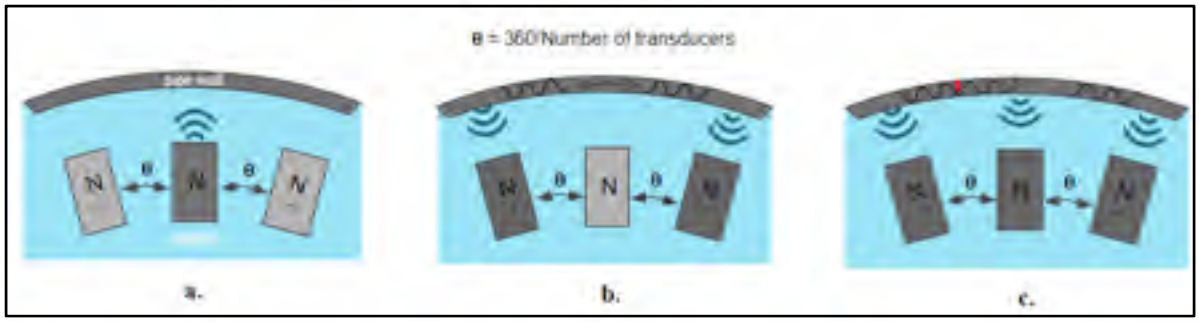

Figure 2.3 Step by step measurement method

2.2 Simulation parameters

To ensure the stability of the simulation, model parameters have to be accurately chosen according to propagating guided wave modes properties.

2.2.1 Elements type

General purpose linear brick elements with reduced integration (of reference C3D8R in Abaqus® and Pogo FEA) were used. These elements represent the best compromise between accuracy and rapidity for ultrasound wave propagation simulations (M. B. Drozdz, 2008).

2.2.2 Elements size

As a FE model is a discretization of a real sample, a compromise must be found between the element size and the computation time. Indeed, reducing elements size will increase computation time and reduce errors made in the simulation, whereas increasing element size will decrease computation time, but wave propagation errors will grow. In the case of wave propagation, the element size is compared with the smallest wavelength to be modelled. Thus,

it was demonstrated that the minimal ratio of elements per wavelength should be close to 10 or 15 (M. Drozdz, Moreau, Castaings, Lowe, & Cawley, 2006). A ratio of 15 will be used in the simulations presented in this thesis.

2.2.3 Time increment

The time increment has to be sufficiently small to prevent the wave to travel through more than a single element during this interval (Cook, 2007). Thereby, to ensure the stability of the simulation, the time increment Δt has to be smaller than the critical time step Δt_{cr} defined as follows by (Cook, 2007) :

$$\Delta t_{cr} = 0.8 \frac{\Delta L}{V_{\Phi_{max}}} \tag{2.1}$$

$V_{\Phi_{max}}$ is the highest phase velocity of the propagating modes, ΔL is the smallest element size and 0.8 is a safety factor.

2.3 Two-dimensional simulation

The transmission of the pressure wave through water and to a cast-iron plate, its conversion to an ultrasonic guided wave in the pipe wall and its reception in the water was first assessed using a two-dimensional (2D) finite element (FE) simulation.

2.3.1 Studied case

As introduce in section 1.1, the choice of the excitation frequency is crucial. A frequency chosen too high will result in a quickly attenuated wave whereas a too low frequency will result in the propagation of very dispersive modes. Additionally, when dealing with pipe modes, a too low frequency will result in the excitation of specific modes that will induce more complexity to the post processing. Knowing that, an excitation frequency centered at 50kHz was selected for both the FE model and experimental study, considering a plate (or a pipe)

made of cast iron ($E = 78.3\ GPa, \rho = 6900\ kg/m^3$ and $\nu = 0.17$), 22 mm thick in order to excite A_0 and S_0 modes below the cutoff frequency of the first high order mode.

2.3.2 Model

As illustrated in Figure 2.4, the model is basically composed of a water layer where the excitation occurs by generating a pressure wave with excitation of several nodes, and a cast iron layer. Both layers are attached together using a tie constraint. Time traces were recorded on nodes located at the surface of the cast iron layer and close to this surface, in the water. The excitation signal was a 5 cycle Hann windowed tone burst centered at 50kHz as shown in Figure 2.5.

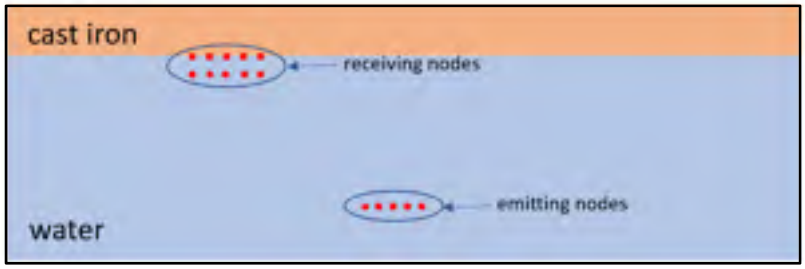

Figure 2.4 Simplified 2D model

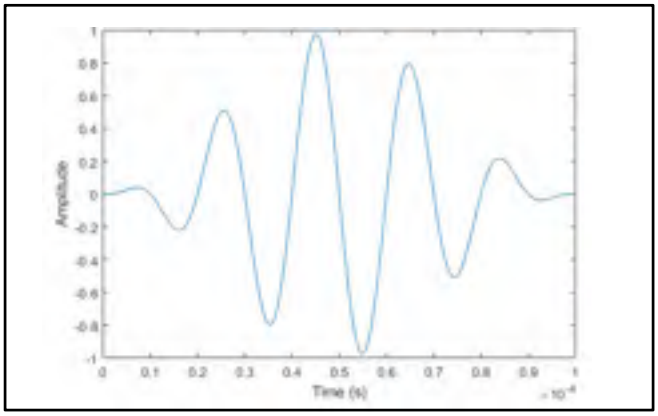

Figure 2.5 Excitation signal. A 50kHz center frequency hann windowed tone burst

2.3.3 Results

First, from the displacement field output, it is interesting to observe the generation and the propagation of the wave in the water and then its transmission in the cast iron layer as shown in Figure 2.6. It is clear that the excited cast iron surface generates an ultrasonic guided wave in the full thickness of this layer. Pressure and stress are represented, respectively for the water and cast-iron layer.

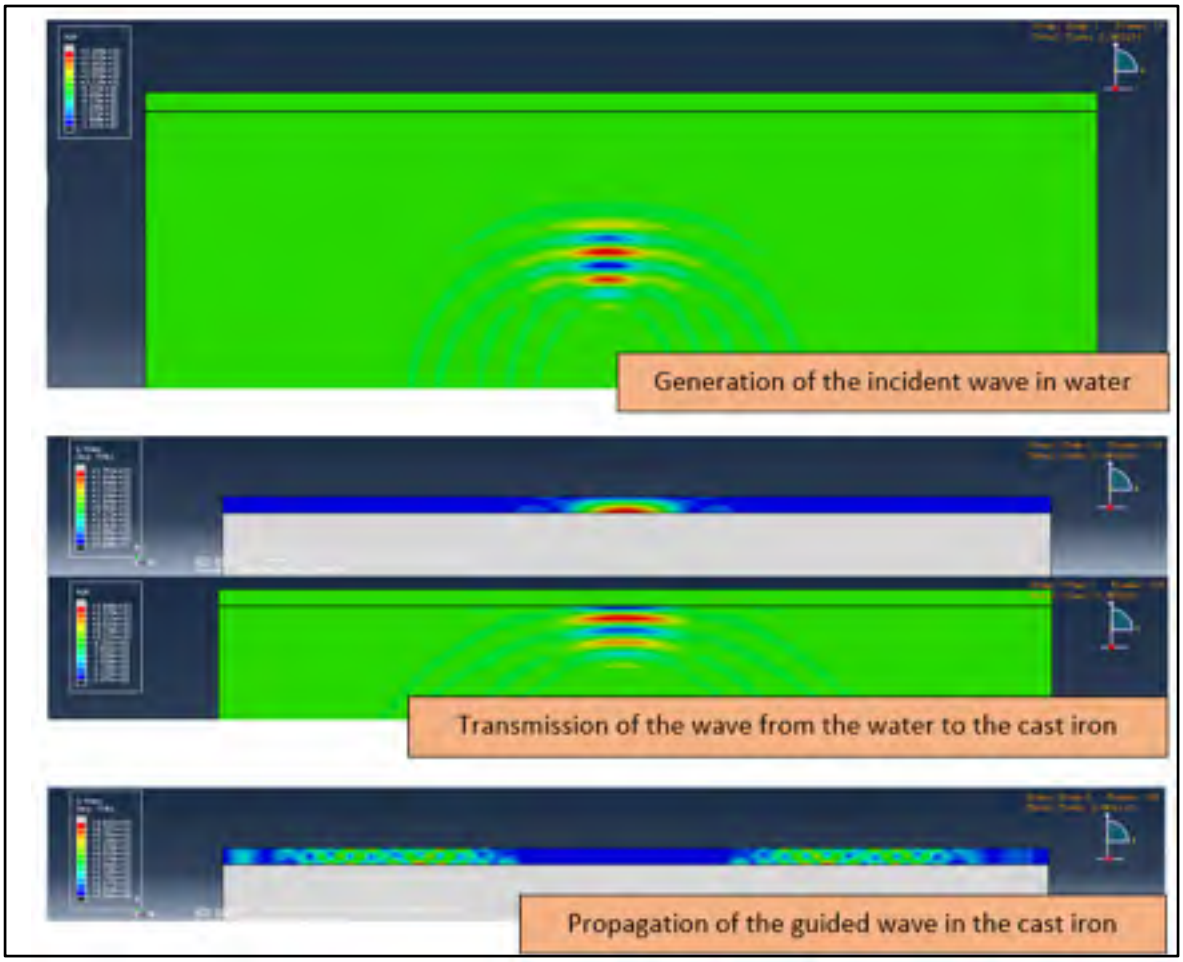

Figure 2.6 Wave propagation in the water and the cast-iron

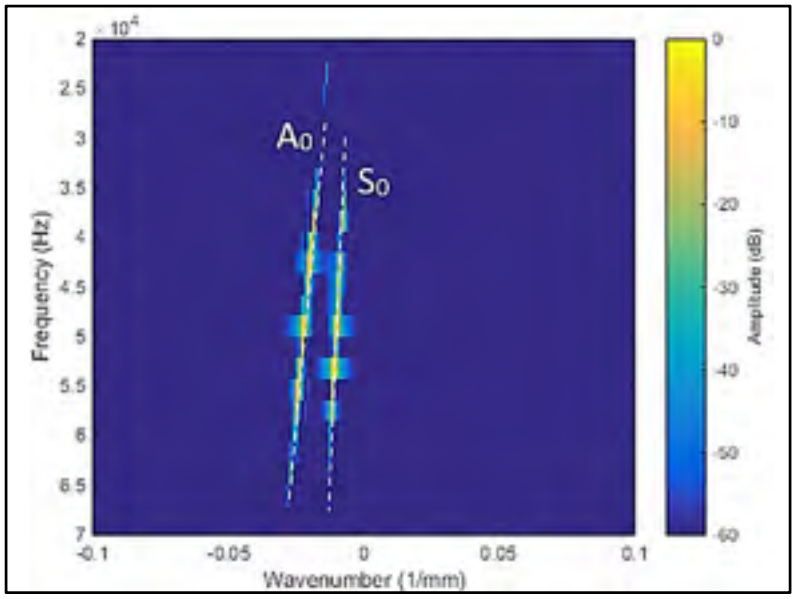

Figure 2.7 Dispersion curves from 2D FFT of measuring nodes displacement showing the propagation of A_0 and S_0 guided waves modes

Then, using time traces recorded at the receiving nodes, it is possible to assess the propagation of excited modes by performing a 2D Fast Fourier Transform (FFT) (Alleyne & Cawley, 1991) and plot dispersion curves in terms of wavenumber and frequency. It is hence easy to identify propagating modes by comparing with dispersion curves provided by GUIGUW. In Figure 2.7, A_0 and S_0 are clearly identified and confirm that the desired modes are propagating in the cast iron layer. However, only A_0 with its strong out-of-plane component that can be measured in water will be exploited for the proposed inspection method.

2.4 Three dimensional simulations

A three-dimensional FE model was then used to asses the proposed inspection method in a 24-inch pipe and along a given axial range. Water was not modeled as it would have resulted in a too large model for our computing resources. Thus, nodes will me excited and monitored directly on the pipe surface as the water coupling was assessed in the previous section. An axial crack was simulated, and the imaging of the pipe is performed using the previously proposed process.

2.4.1 Model

The 3D model, as illustrated in Figure 2.8, aims to reproduce an unbounded section of a 24-inch cast-iron pipe, 22mm thick with a simulated axial crack.

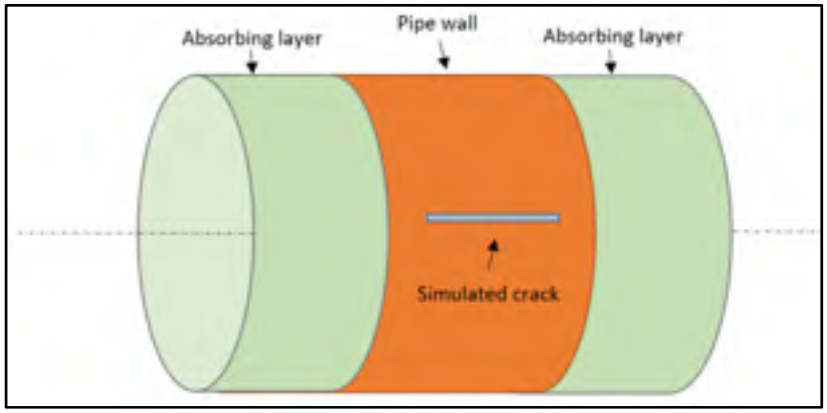

Figure 2.8 Simplified 3D model

Absorbing regions were added on both sides of the pipe using the absorbing layer with increasing damping method (ALID) to avoid reflections from the pipe ends. This method consists in a gradual increase of attenuation coefficient α (see section 1.1.1.4) in the mechanical properties of adjacent layers of elements. The other mechanical properties ($E, \nu \; and \; \rho$) are not changed between each layer. The α coefficient must be increased slightly between each layer to reduce reflections at each interface. The ALID method mathematical development was presented by (M. B. Drozdz, 2008).

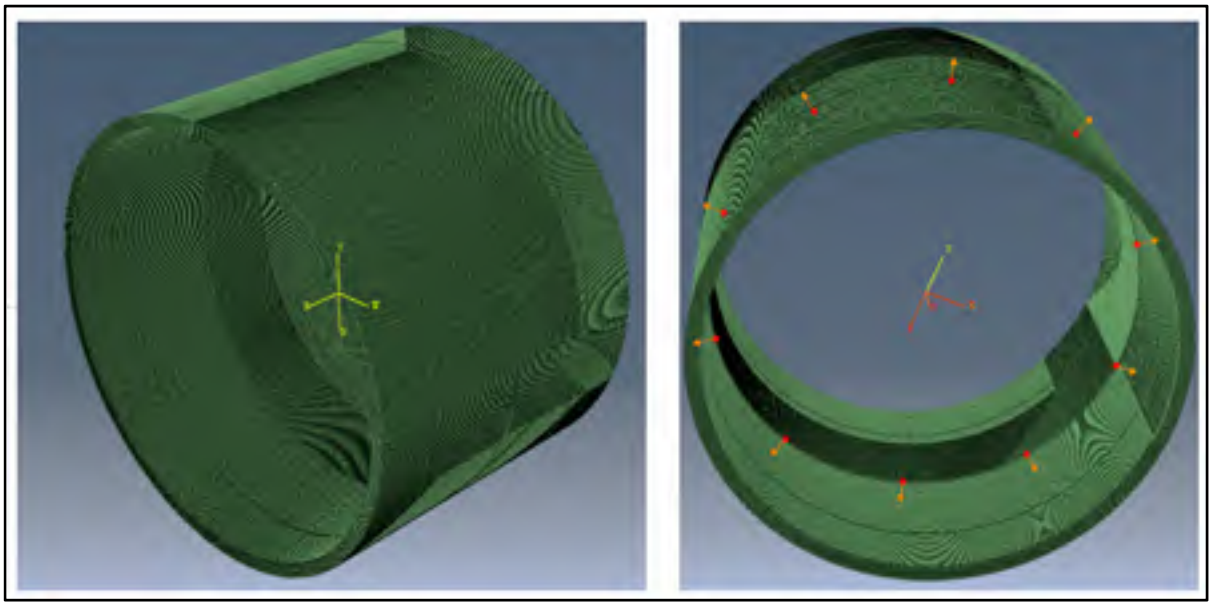

Figure 2.9 3D mesh (left) and 3D mesh with excitation nodes (right)

The simulation replicates the insonification induced by 10 transducers, equally distributed around the pipe circumference (Figure 2.1). Hence, 10 nodes equally distributed around the pipe circumference are excited radially, as illustrated in the right of Figure 2.9, by imposing a force of varying amplitude corresponding to the excitation signal (Figure 2.5). Same material properties than 2D model are used ($E = 78.3\ GPa, \rho = 6900\ kg/m^3$ and $\nu = 0.17$).

Displacement in all directions at excitation nodes was measured for each time step in order to perform the imaging and excitation was sequentially moved along the axial direction to model an in-line inspection. An axial crack of length 224 mm, depth 10 mm from outer surface and width 2 mm was simulated at the center of the model by removing elements.

2.4.2 Results and imaging

Considering an arrangement of 10 transducers corresponding to nodes numbered from 1 to 10 and with a crack located between nodes 3 and 4 as represented in Figure 2.10 a., an example of the received signals (radial displacement) is given in Figure 2.10 b. and Figure 2.10 c.

Signals were post-processed to highlight interesting behavior that will be useful for the back propagation and reconstruction algorithm.

In Figure 2.10 b. the excitation of node 3 was considered but node 3 excitation signal and node 2 direct path signal were removed. Thus, the measurement of node 2 highlights the reflection of the wave from the crack measured at node 2, measurement at node 3 highlights the reflection of the wave from the crack measured at node 3 and finally, measurement at node 4 highlights the direct path of the wave to node 4 that was affected by the crack along its propagation path.

In Figure 2.10 c. the excitation of node 5 was considered but node 4 and 6 direct paths signals were removed. Thus, the measurement of node 4 highlights the reflection of the wave from the crack measured at node 4, the measurement of node 5 highlights the reflection of the wave from the crack measured at node 5 and finally, measurement at node 6 highlights the reflection of the wave from the crack measured at node 6.

Combining all this information with the excitation and the measurement at each node makes it possible to back propagate signals along the pipe circumference in order to generate constructive interferences at the crack circumferential location (Figure 2.11 a.). A single back propagation and summation combination represents a slice of the pipe. This has to be done several times while the PIG is moving to image a given axial range as explained in previous sections. A threshold can be applied to the envelope of the signal (Figure 2.11 a.) and slices assembled to create an image of the pipe wall integrity as shown in Figure 2.11 b.

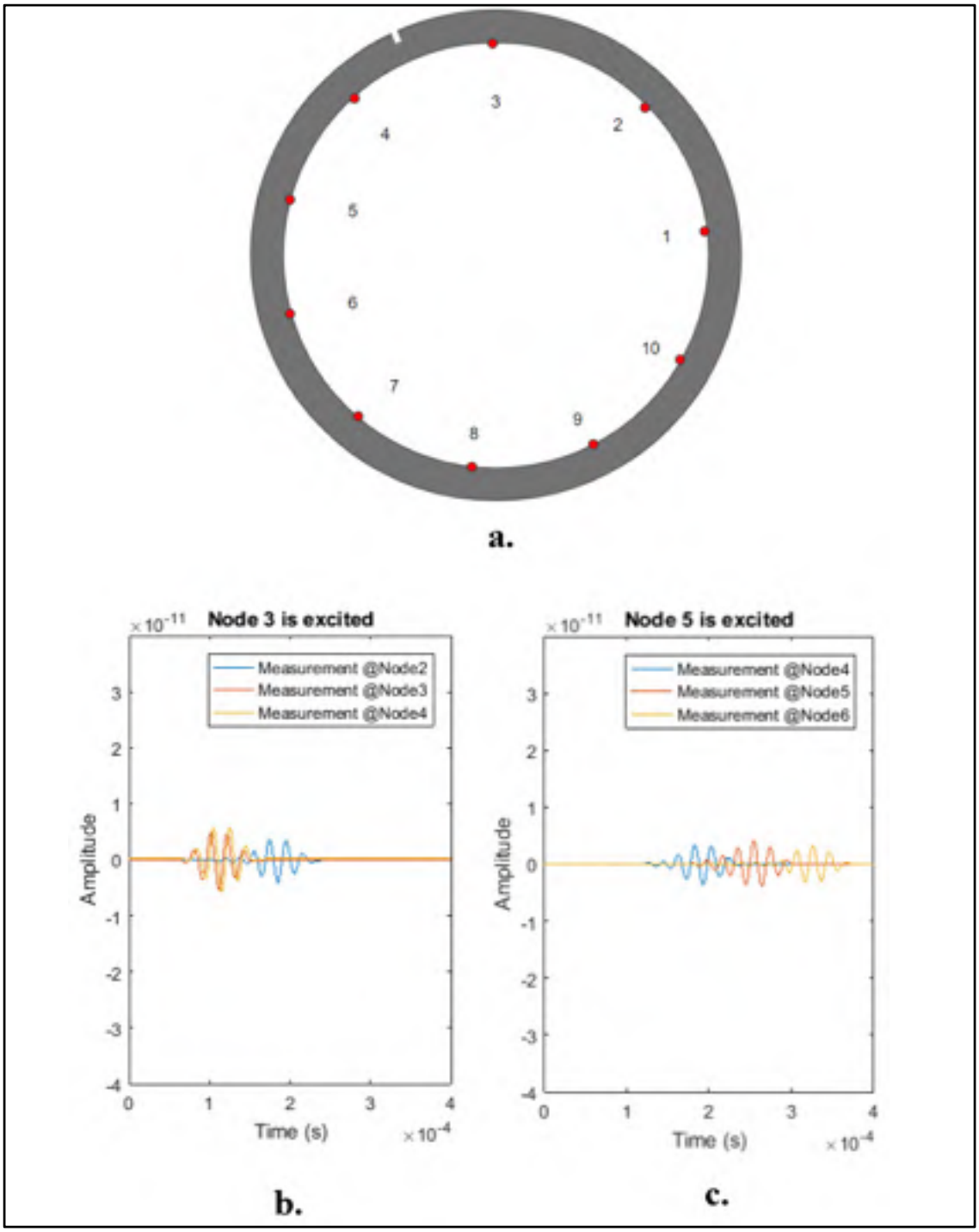

Figure 2.10 a. Measurement setup and crack location. b. Recorded time traces for node 3 excitation where node 3 excitation and node 2 direct path have been removed. c. Recorded times traces for node 5 excitation where node 5 excitation, node 4 and 6 direct path have been removed

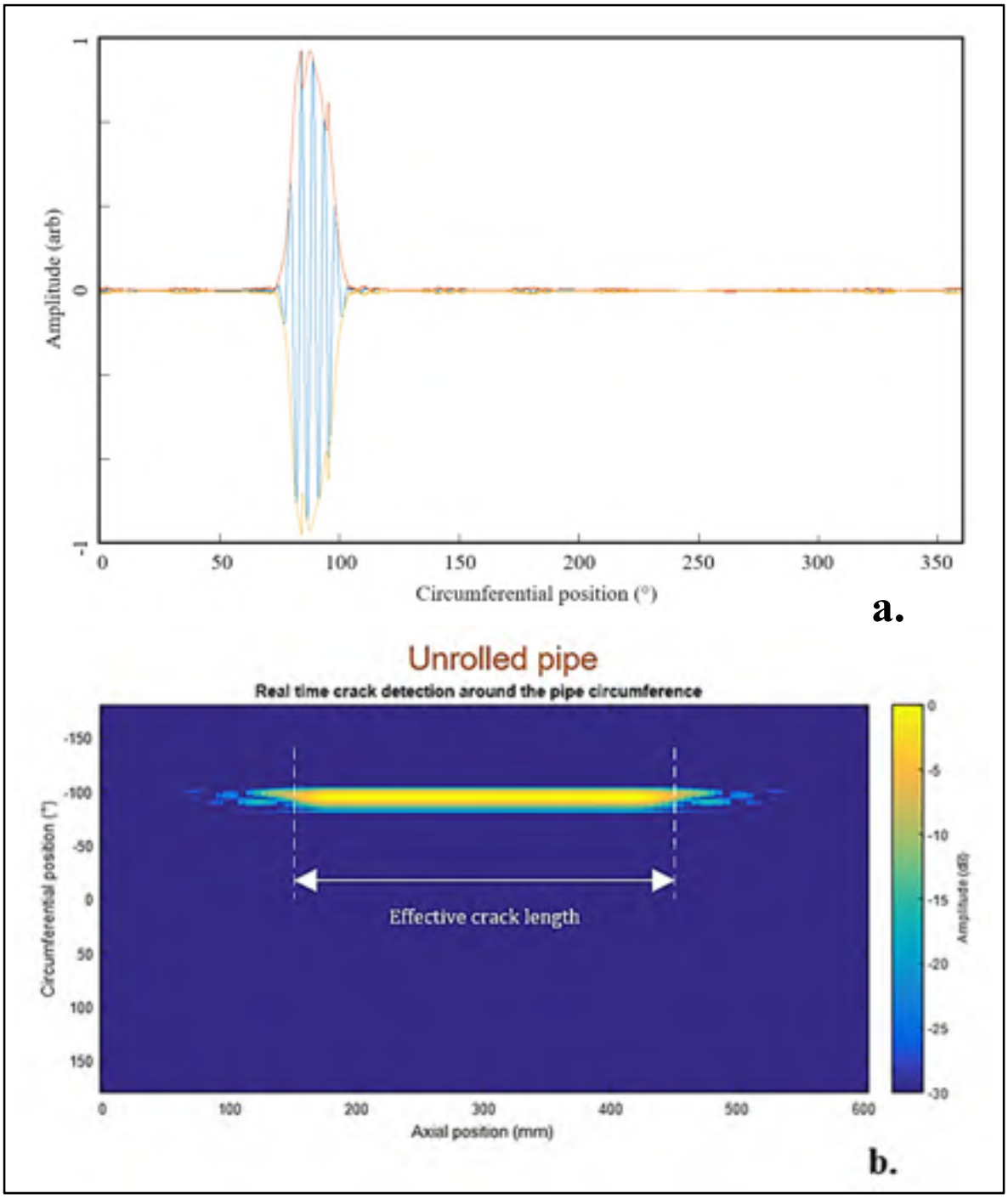

Figure 2.11 a. Summation of back propagated signals for a given slice of the pipe and applied threshold. b. Pipe wall image resulting of the assembly of all slices, simulating an in-line inspection and showing the simulated crack

This simulated inspection (Figure 2.11 b.) corresponds to a PIG speed of 4 m/s and an acquisition time of 4 ms per slice (post-processing time is not considered as it can be done later). The full width at half maximum (FWHM) for the crack extent is of 8 degrees which corresponds to 43 mm for a 24-inch pipe. This is mainly due to signal and crack circumferential extent. The inspection length is 600 mm and 100 slices were used.

2.5 Conclusion on the inspection method and its assessment using FE simulations

The proposed inspection method was presented, the insonification of the pipe through water was tested using a 2D FE model of a similar plate (same thickness and material) and a full inspection of an axial crack using a 3D FE model, limited to the propagation of the wave in the pipe wall due to model size limitations, was performed showing promising results in the final reconstruction image. These results will now be validated against experiments.

CHAPTER 3

EXPERIMENTAL TESTS

The last part of this project was to perform experimental tests to finally assess the feasibility of using ultrasonic guided waves for in-line inspection of cracks in large diameter water pipes.

The industrial partner provided two 24-inch cast-iron pipe (Figure 3.1 a.) samples. One with a cement coating (Figure 3.1 c.) and another one without coating (Figure 3.1 b.). A first experimental test was performed to assess the feasibility of exciting and detecting ultrasonic guided waves in the cement coated sample. Then, custom piezoelectric immersion transducers centered at 50kHz were ordered for tests on a machined groove to reproduce the previously modeled situation. Initial results lead us to proceed to further tests on a cast-iron plate to compare propagation velocities. Finally, in light of the presented results, investigation of another technique using an ultrasonic array transducer is briefly introduced.

Figure 3.1 a. Pipe from which samples have been cut,
b. Non-coated sample and c. Coated sample

3.1 Propagation of guided waves in the coated pipe

A cement coated sample was provided by the industrial partner. This feature was not considered at the beginning of the project, so a first experiment was to assess the propagation of ultrasonic guided waves even in the presence of this coating. Dry and semi-immersed tests were performed.

3.1.1 Dry tests

First, dry tests were performed to assess, on a qualitative basis, that it is possible to guide a wave in the pipe despite the cement coating. A piezoelectric transducer centered at 30kHz was used for the insonification of the pipe, directly coupled to the surface, and the measurement of the propagating wave (i.e. normal displacement at the surface) was performed using a laser Doppler vibrometer (Polytec® OFV-505) using a reflective tape bonded to the pipe surface to increase the signal-to-noise ratio. The measurement setup is shown in Figure 3.2 pictures.

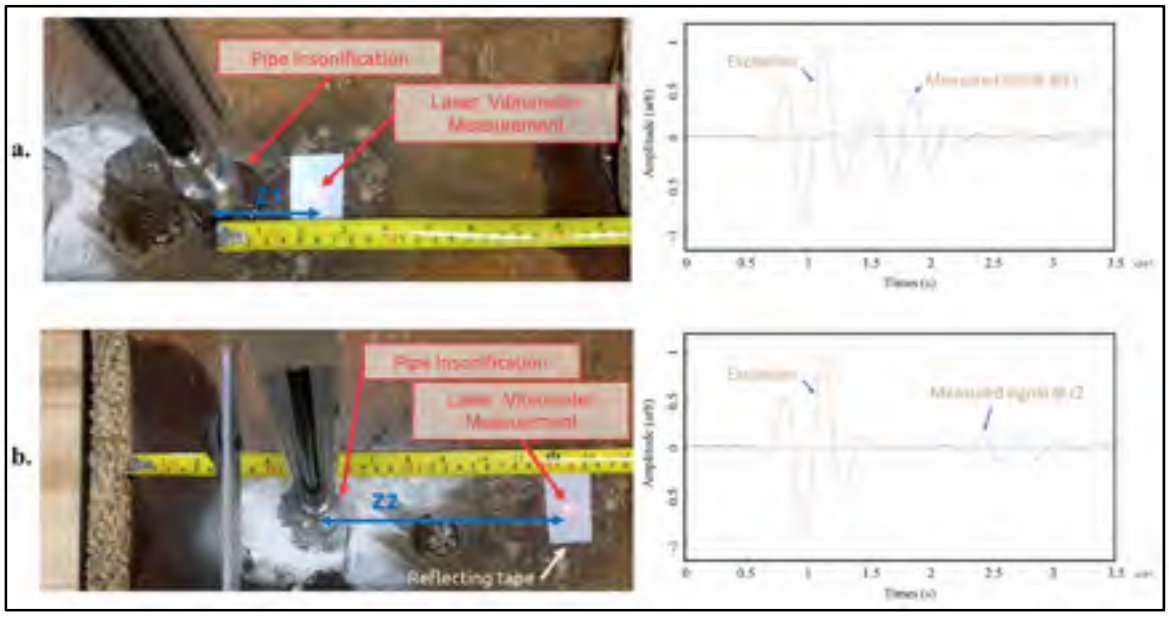

Figure 3.2 Dry tests, a. at a given distance Z1 between the transducer and the laser vibrometer measurement, b. at a given distance Z2 between the transducer and the laser vibrometer measurement. The setup is shown on the left and the emitted and received signal on the right

A 3 cycles Hann-windowed signal generated by an arbitrary waveform generator (Agilent® 33500B) and amplified by a power amplifier (Ritec® RPR-4000) was sent to the transducer. The measured displacement at the pipe surface was first processed by the laser controller (Polytec® OFV-2570) and recorded by on an oscilloscope (Agilent® DSO9024H). Tests were done at two different distances between the transducer and the measurement point to evaluate the repeatability of the experiment.

Results presented in Figure 3.2 shows that the wave is correctly propagating inside the pipe wall despite the cement coating. As expected, the attenuation of the measured signal is observed between time traces of Figure 3.2 a. and Figure 3.2b. due to the greater length of propagation. Additionally, the measured phase velocity of the guided wave is close to 1400 m/s which is less than the expected velocity that should be close to 1750 m/s (according to dispersion curves presented in section 1.1.3).

3.1.2 Semi-immersed tests

Semi-immersed tests were then conducted to assess the through water insonification of the pipe. The cement coated sample was placed in a partially filled 80 gallons water tank (Figure 3.3 a.). The through water insonification was achieved thanks to the same radially oriented transducer and hardware but the input signal was centered at 50 kHz to be closer to the frequency used in the FE model and five cycles were used to reduce the transmitted bandwidth. Finally, the displacement of the pipe surface was measured, on the dry part, using the laser Doppler vibrometer as in the previous subsection.

Results presented in Figure 3.3 b. shows the acquired time traces and Figure 3.3 c. shows the frequency content of the signals. Both figures show that the ultrasonic guided wave is correctly propagating inside the pipe wall despite the water coupling and the cement coating. Dispersion and close boundaries of the pipe are responsible of the elongated shape of the received signal. The frequency content is also slightly affected.

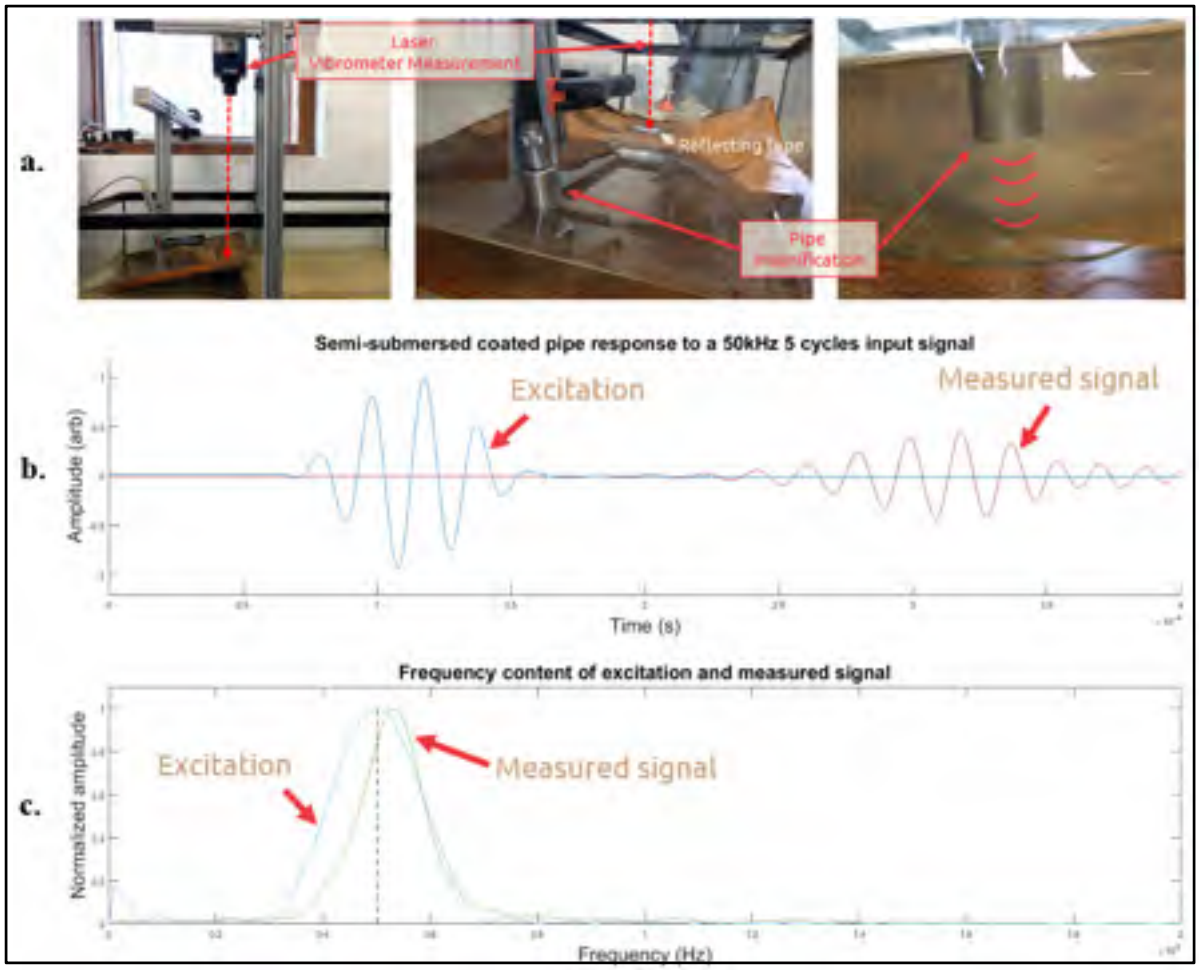

Figure 3.3 Semi-immersed tests, a. Experimental setup, b. Emitted and measured signal, c. Frequency content of the emitted and received signal

3.2 Inspection of a machined groove and first conclusions

Custom 50kHz centered immersion transducers were then used to achieve an inspection similar to the previously simulated case. Thus, a groove 50% deep was machined in the pipe wall and transducers immersed in the water were used both for the emission and reception of the wave. Transducers were mounted on a motorized axis to control their movement along the pipe axial direction. Due to a disappointing behavior during first tests, a series of troubleshooting tests were done in order to understand the observed results.

3.2.1 Inspection of a machined groove reproducing the simulated case

As introduced, a groove was machined on the pipe surface as shown in the left picture of Figure 3.4 where the groove dimensions are also reported. The same experimental hardware and signal processing as in section 3.1.2 was used for the insonification of the pipe using the 50 kHz transducers and a receiver was used to amplify the signal coming from the receiving transducer. In this experimental setup (Figure 3.4), a second transducer (2) is used to achieve the pulse-echo measurement (instead of the emitting transducer 1) due to device limitations with the amplifier and diplexer.

According to simulations results, the expected behavior is as follows:

- When the setup (right picture in Figure 3.4) is not above the groove and transducer 1 is fired:
  - Transducer 2 measures the guided wave going from 1 to 3.
  - Transducer 3 measures the guided wave coming from 1.
- When the setup is above the groove and transducer 1 is fired:
  - Transducer 1 measures a reflection from the groove.
  - Transducer 2 measures the guided wave going from 1 to 3 and a reflection from the groove.
  - Transducer 3 measures the guided wave from 1 at a lower amplitude than the previous case.

Figure 3.4 Measurement setup for the inspection of the groove

But unfortunately, the observed behavior was as follows:

- When setup was not above the groove and transducer 1 was fired:
    - Transducer 2 measured the wave which was propagating in the water from 1 to 3.
    - Transducer 3 measured the wave which was propagating in the water and coming from 1.
- When setup was above the groove and transducer 1 was fired:
    - Transducer 1 didn't measure a reflection from the groove due to device limitation (amplifier/diplexer).
    - Transducer 2 measured the wave which was propagating in the water from 1 to 3.
    - Transducer 3 measured the wave which was propagating in the water and coming from 1.

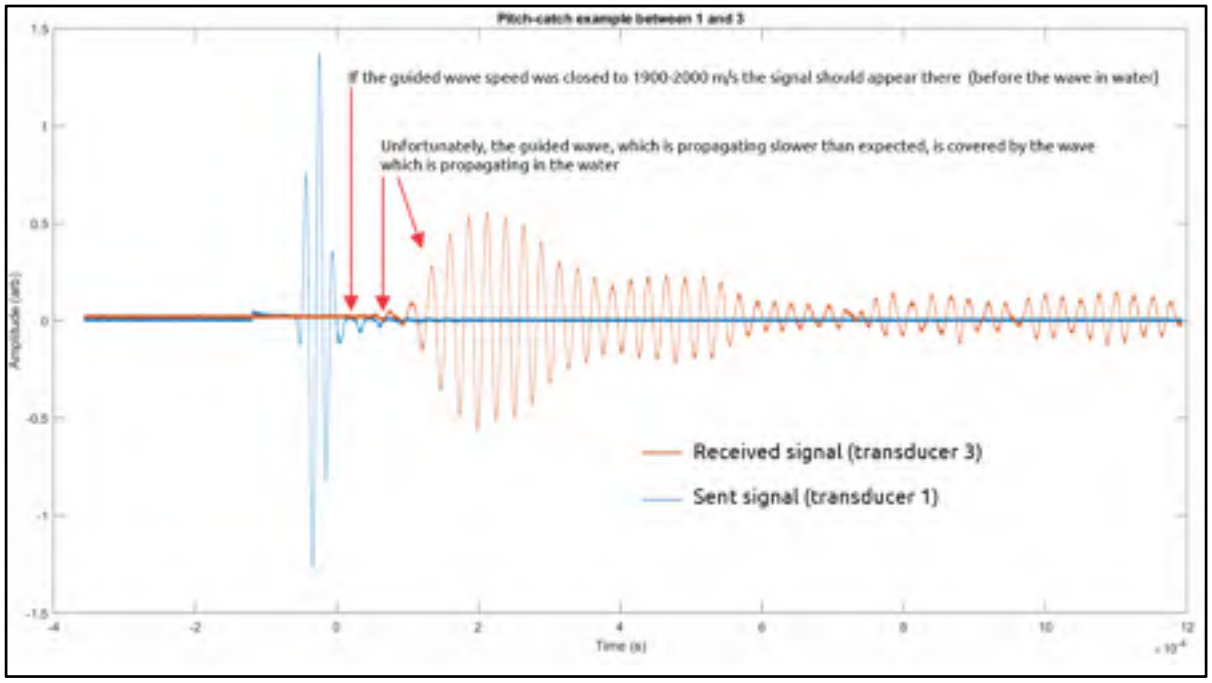

Figure 3.5 Pitch-catch example of observed signals, transducer 1 is fired and signal is measured by transducer 3.

This unexpected behavior can actually be explained simply. Indeed, according to time traces shown in Figure 3.5 where the emitted signal at transducer 1 and its reception at transducer 3 is plotted, it appears clearly that the reception of the guided wave was completely masked by the pressure wave which was propagating in the water. If the ultrasonic guided wave was propagating much faster than the pressure wave in the water (velocity of 1480 m/s), then the ultrasonic guided wave would have appeared earlier on this same time trace. Thus, unexpected material properties are mainly responsible for this behavior. However, this will be confirmed by the next experiment.

3.2.2 Measurement of the ultrasonic guided wave velocity in a simple cast-iron plate

The previous experiment has planted a seed of doubt on the feasibility of the proposed method. The idea behind the experiment in this subsection is to compare the previously observed behavior with a different cast-iron sample. Thus, a cast-iron plate of width 10 inches, length 15 inches and half an inch thick was used to conduct pitch-catch measurements. The excitation frequency, hardware and transducers were the same as for the pipe groove experiments. The setup is presented in Figure 3.6. The plate was immersed in water as well as the transducers A and B that were spaced by 203 mm and placed at 2 mm above the plate.

Figure 3.6 Measurement setup for pitch-catch tests on a cast-iron plate.

Results obtained for a pitch-catch measurement are presented in Figure 3.7. Figure 3.7 a. shows that the ultrasonic guided wave can be distinguished from the wave propagating in the water

because of its earlier arrival. A more detailed time trace of the received ultrasonic guided wave signal is shown in Figure 3.7 b. which allows to calculate the phase velocity of the wave which was close to 1980 m/s. Hence, using a different cast-iron sample, which is supposed to have the same (or close) properties, the phase velocity of the guided wave for the same frequency is much higher. It shouldn't be forgotten that the waveguide thickness is also important for the propagation velocities.

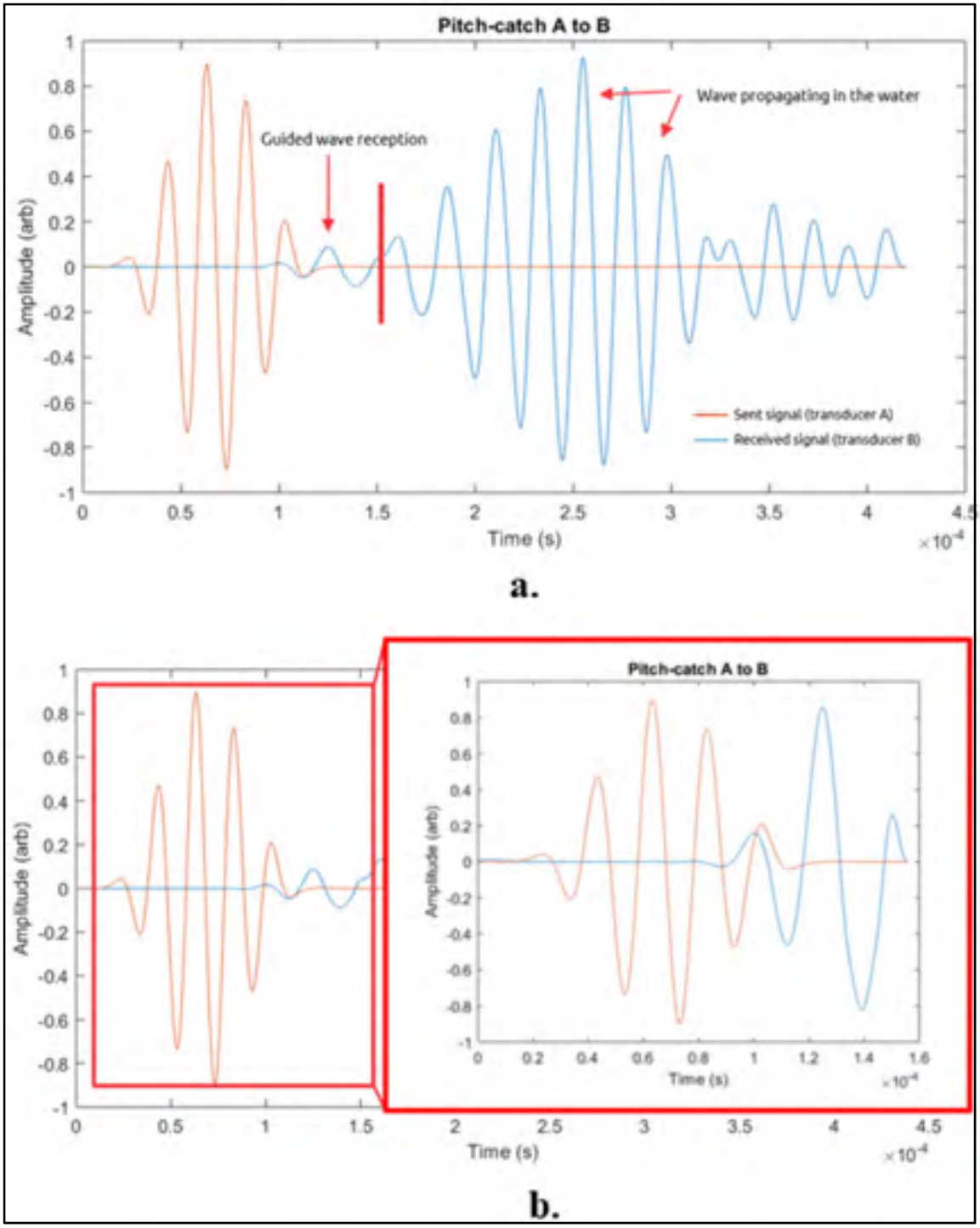

Figure 3.7 Pitch-catch measurement from transducer A to B

3.2.3 Measurement of the guided wave speed in the pipe using transduction on each side of the pipe

Finally, a precise velocity measurement of the guided wave propagating in the pipe sample for a frequency of 50 kHz and in the fully immersed case was conducted. In order for the guided wave propagating in the pipe wall not to be masked by the pressure wave in the water, the insonification of the pipe was performed from the inside of the pipe sample and the measurement of the propagating wave was performed from the outside of the pipe sample. The measurement setup is presented in Figure 3.8 a. where transducer 1 is used for emission and transducers 2 and 3 for reception. They were located at 2 mm from the pipe surface and the same signal and hardware was used as in the previous experiment. Figure 3.8 b. shows the signal sent to transducer 1 and received signal at transducer 2. Transducer 3 is used to confirm transducer 2 measurement. A phase velocity close to 1560 m/s was measured. It is consistent with the first phase velocity measurement of section 3.1.1. In addition, this velocity is very close to the one of pressure wave in water, 1480 m/s, which explain the previously observed behavior.

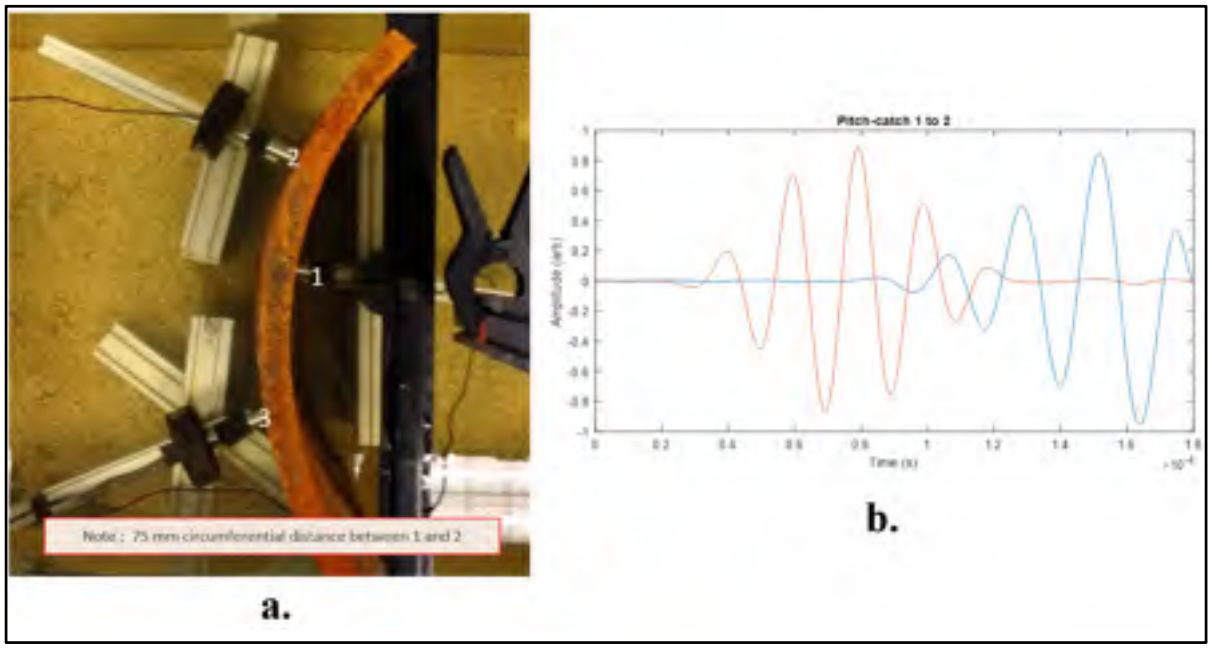

Figure 3.8 a. Measurement setup for the guided wave phase velocity measurement.
b. Signals sent to transducer 1 and received by transducer 2

3.2.4 First conclusions on the feasibility of the proposed method

Several tests were carried out to assess the experimental feasibility of the proposed method introduced in CHAPTER 2. Multiple unexpected parameters such as the cement coating and variable material properties of cast-iron were the main challenges. Unfortunately, even if it is possible to propagate ultrasonic guided wave in the cement coated sample using water as couplant, fully immersed tests were disappointing due to a phase velocity too close to the pressure wave in water, resulting in completely masked ultrasonic guided wave signals.

Hence, materials properties of the provided cast-iron pipe sample were the main drawback to the use of this method. A higher frequency shouldn't be used due to the propagation of higher order modes which would involve a much more complicated signal post-processing. A lower frequency will lead to a slower phase velocity and the same issue with the pressure wave propagating in water.

3.3 Use of an ultrasonic array

During the last weeks of this project, a completely different approach was tested using an ultrasonic array to perform the in-line inspection using bulk waves, which propagate at a much higher velocity, instead of ultrasonic guided waves. Additionally, array transducers enable the formation of precise images of the pipe wall.

The Verasonics® Vantage ™ research ultrasound system was used in combination with a Philips® L7-4 128 elements medical linear array of aperture 38 mm to emit and receive plane waves in water in order to image the pipe wall.

A longer groove was machined on the inner surface of the pipe as well as an outer groove as shown in Figure 3.9. They were both 50% deep.

Figure 3.9 Machined grooves on inner and outer surfaces of the pipe sample

The linear array was attached to a motorized linear stage located above the water tank and tests were performed for different probe to pipe surface distances (20mm, 100mm, and 170mm). The array was perpendicular to the groove direction as shown in Figure 3.10. for both the inner and outer groove.

Figure 3.10 Array setup above the groove under inspection

Plane waves were emitted directly under the probe aperture but also at different angles using delays in order to increase the covered circumferential extent. Different encouraging results are shown in Figure 3.11.

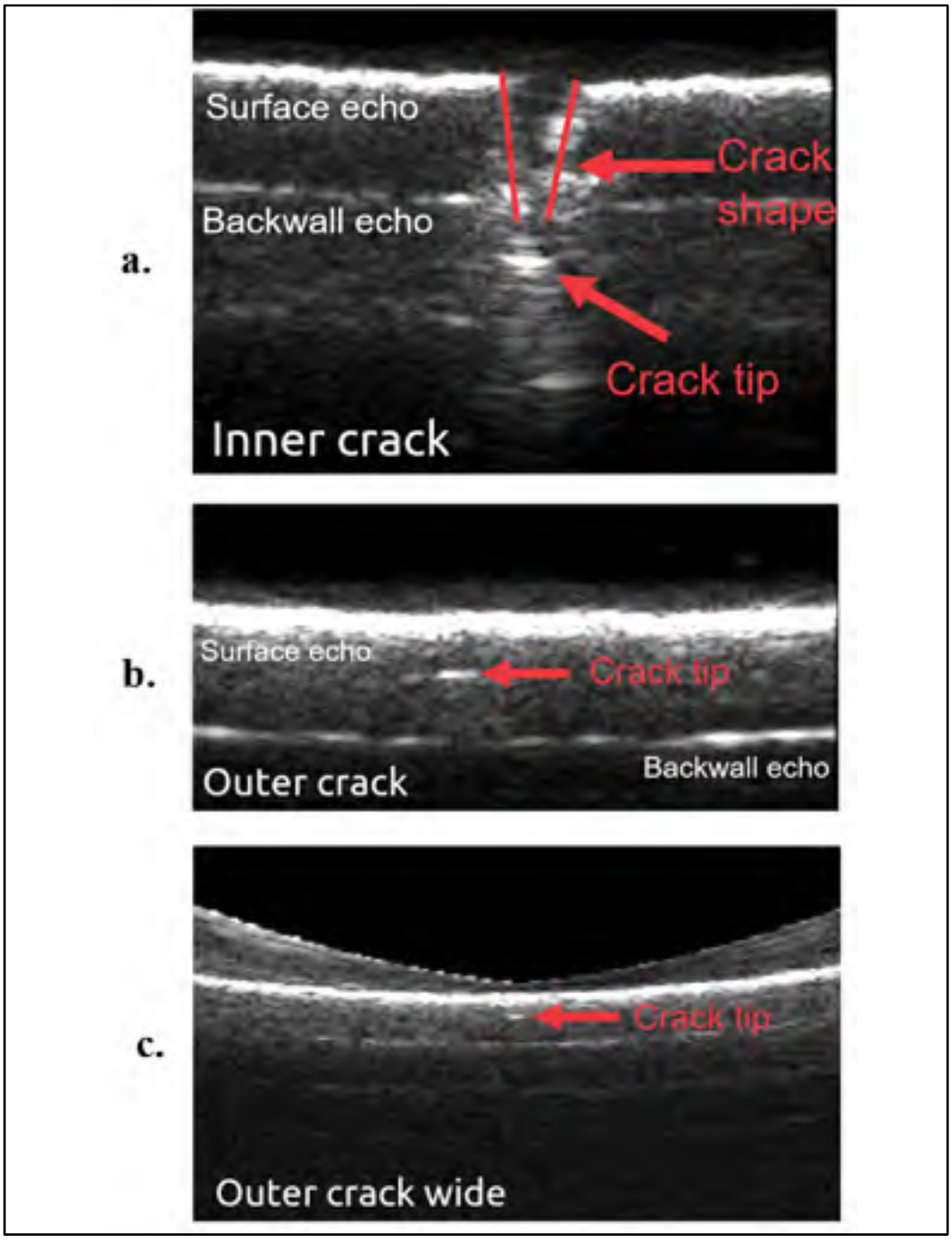

Figure 3.11 Imaging results using the linear array. a. 100mm from the pipe surface. Image of the inner groove. Image width corresponds to probe aperture. b. 20 mm from the pipe surface. Image of the outer groove. Image width correponds to the probe aperture. c. 170 mm from the pipre surface. Image of the outer groove. Image corresponds to a 90 mm circumferential extent

Figure 3.11 a. shows an acquisition performed above the inner groove. The distance between the probe and the pipe surface was 100 mm. The surface as well as the backwall echoes were clearly distinguished and the pipe thickness was fully imaged. The image width corresponded to the 38 mm probe aperture. In this setup, the groove was partially (half thickness) filled with water. As mentioned in previous sections, the velocity of pressure waves in water is 1480 m/s which is far less than bulk waves in cast iron (approximately 5000 m/s). Thus, the crack tip appears bellow the backwall echo. The crack shape was also clearly visible.

Figure 3.11 b. shows an acquisition performed above the outer groove at 20 mm from the pipe surface. Surface and backwall echoes were also clearly visible as well as the crack tip of the groove. This time, there were no delay imposed by the velocity of the wave in the water because the wave is directly transmitted into the pipe at its interface with water.

Finally, Figure 3.11 b shows a wider image of the pipe surface when the setup was above the outer groove at a distance of 170 mm. Plane waves at different angles were sent to image up 90 mm of circumference of the pipe. Once again, surface, backwall and crack tip echoes were clearly visible.

These results are very encouraging and could be improved by an extensive work using this technique, especially by enhancing the reconstruction algorithm but also by using a phased array probe. Angular insonification could be studied for crack sizing in a similar way to how welds are inspected. Using multiple probes and appropriate hardware will lead to the full circumference coverage.

CONCLUSION

The proposed inspection method had the main advantage of being a low-cost solution to the in-line inspection of axial cracks in cast-iron water pipes. It used a small number of inexpensive transducers and a simple and fast reconstruction algorithm that was tested using FE simulations. Unfortunately, despite the good capabilities of cast iron to support the propagation of ultrasonic guided waves using water as couplant, even with a cement coating, pressure wave in water was hindering the detection of ultrasonic guided waves propagating in the pipe wall of the provided sample.

Thus, disparity of cast iron material properties was the main drawback to the use of this method. The use of a higher excitation frequency shouldn't be considered as it would involve the propagation of higher order modes and complex signal processing. Using a lower frequency is also not possible because it will lead to a slower phase velocity and the same issue with the pressure wave propagating in water.

An encouraging method was finally tested, using ultrasonic array transducers. Array transducers enable the formation of images of the pipe wall. Initial results are very promising, and this work will be continued in a new master project. However, this solution is way more expensive and generate a huge amount of data that has to be processed.

Further studies will also have to be conducted on the inspection of the bell and spigot joint, which is the part of the pipe where the initiation of a crack is often observed due to thermal expansion coefficient disparity between the joint and the bell medium. The presented method proved to be inadequate to inspect this part of the pipe due to the complex geometry of the bell but the use an ultrasonic array should also be investigated.

BIBLIOGRAPHY

Alleyne, D., & Cawley, P. (1991). A two-dimensional Fourier transform method for the measurement of propagating multimode signals. *J Acoust Soc Am, 89*(3), 1159-1168. doi: 10.1121/1.400530

American Water Works Service Co, I. A. (2002). Deteriorating Buried Infrastructure Management Challenges and Strategies. *United States Environmental Protection Agency*.

Atkinson, K., Whiter, J. T., Smith, P. A., & Mulheron, M. (2002). Failure of small diameter cast iron pipes. *Urban Water, 4*(3), 263-271. doi: https://doi.org/10.1016/S1462-0758(02)00004-3

Auld, B. A. (1973). *Acoustic fields and waves in solids*. New York,: Wiley.

Berdin, C., Dong, M. J., & Prioul, C. (2001). Local approach of damage and fracture toughness for nodular cast iron. *Engineering Fracture Mechanics, 68*(9), 1107-1117. doi: https://doi.org/10.1016/S0013-7944(01)00010-8

Bocchini, P., Marzani, A., & Viola, E. (2011). Graphical User Interface for Guided Acoustic Waves. *Journal of Computing in Civil Engineering, 25*(3), 202-210. doi: 10.1061/(ASCE)CP.1943-5487.0000081

Cawley, P., Lowe, M., Alleyne, D., Pavlakovic, B., & Wilcox, P. (2003). Practical long range guided wave inspection-applications to pipes and rail. *Mater. Eval, 61*(1), 66-74.

Cheeke, J. D. N. (2012). *Fundamentals and applications of ultrasonic waves* (2nd éd.). Boca Raton, Fla.: CRC Press.

Cook, R. D. (2007). *Concepts and applications of finite element analysis*. John wiley & sons.

Dieulesaint, E., & Royer, D. (1980). *Elastic waves in solids : applications to signal processing*. Chichester Eng. ; New York: J. Wiley.

Drozdz, M., Moreau, L., Castaings, M., Lowe, M. J. S., & Cawley, P. (2006). Efficient Numerical Modelling of Absorbing Regions for Boundaries Of Guided Waves Problems. *AIP Conference Proceedings, 820*(1), 126-133. doi: 10.1063/1.2184520

Drozdz, M. B. (2008). *Efficient Finite Element Modelling of Ultrasound Waves in Elastic Media*. University of London.

Felli, F., & Lupi, C. (2016). Critical Issues on Cast Iron Pipelines. *Procedia Structural Integrity, 2*, 2966-2973. doi: https://doi.org/10.1016/j.prostr.2016.06.371

Feng, Q., Li, R., Nie, B., Liu, S., Zhao, L., & Zhang, H. (2017). Literature Review: Theory and Application of In-Line Inspection Technologies for Oil and Gas Pipeline Girth Weld Defection. *Sensors (Basel, Switzerland), 17*(1), 50. doi: 10.3390/s17010050

Huadong, S., Liang, Y., Guangheng, L., Guiyun, T., Denis, O., Yunpeng, S., & Shangqing, L. (2018). Comparative Analysis of In-line Inspection Equipments and Technologies. *IOP Conference Series: Materials Science and Engineering, 382*(3), 032021.

Huthwaite, P. (2014). Accelerated finite element elastodynamic simulations using the GPU. *Journal of Computational Physics, 257*, 687-707. doi: https://doi.org/10.1016/j.jcp.2013.10.017

Lamb, H. (1917). On waves in an elastic plate. *Proceedings of the Royal Society of London. Series A, 93*(648), 114-128. doi: 10.1098/rspa.1917.0008

Leinov, E., Cawley, P., & Lowe, M. J. S. (2014). Investigation of guided waves propagation in pipe buried in sand. *AIP Conference Proceedings, 1581*(1), 271-278. doi: 10.1063/1.4864830

Li, J., & Rose, J. L. (2006). Natural beam focusing of non-axisymmetric guided waves in large-diameter pipes. *Ultrasonics, 44*(1), 35-45. doi: https://doi.org/10.1016/j.ultras.2005.07.002

M. Beller, K. R. (2002). Tools, Vendors, Services: A Review of Current In-Line Inspection Technologies. *Pipeline Pigging, Integrity Assessment, and Repair Conference, Houston*.

Makar, J. M. (2000). A preliminary analysis of failures in grey cast iron water pipes. *Engineering Failure Analysis, 7*(1), 43-53. doi: https://doi.org/10.1016/S1350-6307(99)00005-9

Makar, J. M., Desnoyers, R., & McDonald, S. E. (2001). Failure modes and mechanisms in gray cast iron pipe. 1-10.

Pavlakovic, B., Lowe, M., Alleyne, D., & Cawley, P. (1997). *DISPERSE: A general purpose program for creating dispersion curves* (Vol. 16). doi: 10.1007/978-1-4615-5947-4_24

Rajani, B., Zhan, C., & Kuraoka, S. (1996). Pipe soil interaction analysis of jointed water mains. *Canadian Geotechnical Journal, 33*(3), 393-404. doi: 10.1139/t96-061

Reber, K., Beller, M., Willems, H., & Barbian, O. A. (2002). A new generation of ultrasonic in-line inspection tools for detecting, sizing and locating metal loss and cracks in transmission pipelines. Dans *2002 IEEE Ultrasonics Symposium, 2002. Proceedings.* (Vol. 1, pp. 665-671 vol.661). doi: 10.1109/ULTSYM.2002.1193490

Rezaei, H., Ryan, B., & Stoianov, I. (2015). Pipe Failure Analysis and Impact of Dynamic Hydraulic Conditions in Water Supply Networks. *Procedia Engineering, 119*, 253-262. doi: https://doi.org/10.1016/j.proeng.2015.08.883

Rose, J. L. (2014). *Ultrasonic Guided Waves in Solid Media*. Cambridge: Cambridge University Press. doi: 10.1017/CBO9781107273610

Royer, D., & Dieulesaint, E. (1996). *Ondes élastiques dans les solides*. Paris: Masson.

Solie, L. P., & Auld, B. A. (1973). Elastic waves in free anisotropic plates. *J Acoust Soc Am, 54*(1), 50-65. doi: 10.1121/1.1913575

Willems, H., Jaskolla, B., Sickinger, T., Barbian, A., & Niese, F. (2010). A New ILI Tool for Metal Loss Inspection of Gas Pipelines Using a Combination of Ultrasound, Eddy Current and MFL. (44205), 557-564. doi: 10.1115/IPC2010-31387